

FUSION: Forecast-Embedded Agent Scheduling with Service Incentive Optimization over Distributed Air-Ground Edge Networks

Houyi Qi, Minghui Liwang, *Senior Member, IEEE*, Seyyedali Hosseinalipour, *Senior Member, IEEE*, Liqun Fu, *Senior Member, IEEE*, Sai Zou, *Senior Member, IEEE*, Xianbin Wang, *Fellow, IEEE*, Wei Ni, *Fellow, IEEE*, and Yiguang Hong, *Fellow, IEEE*

Abstract—In this paper, we introduce a first-of-its-kind forecasting-driven, incentive-inherent service provisioning framework for distributed air-ground integrated networks that explicitly accounts for human-machine coexistence. In our framework, vehicular-UAV agent pairs (APs) are proactively dispatched to overloaded hotspots to augment the computing capacity of edge servers (ESs), which in turn gives rise to a set of challenges that we jointly address: highly uncertain spatio-temporal workloads, spatio-temporal coupling between road traffic and UAV capacity, forecast-driven contracting risks, and heterogeneous quality-of-service (QoS) requirements of human users (HUs) and machine users (MUs). To address these challenges, we propose FUSION, a two-stage optimization framework, consisting of an offline stage and an online stage. In the offline stage, a liquid neural network-powered module performs multi-step spatio-temporal demand forecasting at distributed ESs, whose outputs are exploited by an enhanced ant colony optimization-based routing scheme and an auction-based incentive-compatible contracting mechanism, to jointly determine ES-AP contracts and pre-planned service routes. In the online stage, we formulate the congestion-aware task scheduling as a potential game among HUs, MUs, and heterogeneous ES/UAVs, and devise a potential-guided best-response dynamics algorithm that provably converges to a pure-strategy Nash equilibrium. Experiments on both synthetic and real-world datasets show that FUSION consistently achieves higher social welfare and improved resource utilization, while maintaining latency and energy costs comparable to state-of-the-art baselines and preserving individual rationality, budget balance, and near-truthfulness.

Index Terms—Distributed edge computing, liquid neural network, auction, potential games, heterogeneous network users.



1 INTRODUCTION

Recent years have witnessed a new generation of intelligent applications such as real-time distributed video analytics, intelligent transportation systems, and large-scale mobile crowdsensing, flourishing across smart cities [1], [2]. Although edge servers (ESs) can provide computing capabilities for these intelligent applications at the network edge, their limited local resources make them susceptible to resource shortages and task congestion during peak demand periods [3].

To address the limitations of ESs, low-altitude edge computing enabled by unmanned aerial vehicles (UAVs) has received significant attention [4], [5]. Unlike static ESs, UAVs provide high mobility and flexibility, allowing them to be rapidly dispatched to hotspot regions to provide the needed computing resources. In this work, we highlight an important yet often-overlooked aspect of low-altitude edge systems: most existing studies implicitly assume that UAVs can always *fly directly* to target regions [6]–[9], without considering their deployment origins. This is despite the fact that long travel

distances due to poorly planned deployment origins can easily deplete UAVs’ batteries before reaching target locations. To fill this gap, we propose an *air-ground cooperative edge computing paradigm*: during periods of intensive demand, a set of ground vehicles are used to transport UAVs (vehicles and UAVs are collectively referred to “agent pairs (APs)”) to the vicinities of overloaded ESs. UAVs are then launched from strategically selected locations to deliver temporary computational augmentation for ESs. Despite its promising potential, operationalizing this hybrid AP-ES deployment paradigm introduces several challenges, which must be addressed:

(A) Spatio-temporal demand uncertainty. Edge computing demands exhibit strong spatio-temporal variability, and the coexistence of human users (HUs) and machine users (MUs) further complicates the management of distributed workloads. This variability makes it difficult to determine when, where, and how UAV resources should be dispatched. In such networks, static provisioning or purely reactive scheduling often leads to mismatches between supply and demand, resulting in congestion at emerging hotspots and resource underutilization in low-demand regions [12], [13]. The key challenge therefore lies in accurately forecasting spatio-temporal demand patterns from historical requests and contextual information, so as to enable proactive UAV deployment.

(B) Spatio-temporal coupling of vehicular mobility and UAV deployment. Supporting geo-distributed ESs requires APs to rely on vehicular mobility to reach target locations, which is constrained by road topology and traffic conditions. Moreover, the number of UAVs that can be deployed by a vehicle is tightly coupled with its visiting sequence and dwell

H. Qi (houyiqi@tongji.edu.cn), M. Liwang (minghuiliwang@tongji.edu.cn), and Y. Hong (yghong@iss.ac.cn) are with the Shanghai Research Institute for Intelligent Autonomous Systems, with the State Key Laboratory of Autonomous Intelligent Unmanned Systems, Frontiers Science Center for Intelligent Autonomous Systems, Ministry of Education, Shanghai Key Laboratory of Intelligent Autonomous Systems, and Department of Control Science and Engineering, Tongji University, China. S. Hosseinalipour (alipour@buffalo.edu) is with Department of Electrical Engineering, University at Buffalo-SUNY, USA. L. Fu (liqun@xmu.edu.cn) is with School of Informatics, Xiamen University, China. S. Zou (dr-zousai@foxmail.com) is with College of Big Data and Information Engineering, Guizhou University, China. X. Wang (xianbin.wang@uwo.ca) is with the Department of Electrical and Computer Engineering, Western University, Canada. W. Ni (Wei.Ni@ieee.org) is with Data61, CSIRO, Sydney, Australia.

time at each ES, since UAV dispatching, service execution, and recovery jointly consume time and onboard resources. Consequently, vehicle-UAV joint deployment becomes a highly coupled optimization problem that must simultaneously account for travel costs, service time windows, UAV dispatching logistics, and spatially distributed service rewards.

(C) Predictive contracting and incentive-compatible trading. In the ES-AP hybrid network, APs operated by private entities must be compensated by ES operators through *advance contracts* that commit service capacity and pricing for future peak-demand periods before demand realization. However, forecasting errors and dynamic supply-demand variations introduce significant risks for both parties: ESs may suffer unmet demand, while APs may incur revenue loss due to resource misallocation. The central challenge is thus to design a reliable offline trading mechanism that is individually rational, incentive compatible, and budget feasible, while operating prior to demand realization and service execution [14].

(D) Online network coordination under human-machine coexistence. HUs and MUs compete for shared resources provided by local ESs and leased UAVs, yet exhibit fundamentally different QoS requirements. HUs are typically delay-sensitive due to interactive applications, whereas MUs emphasize timely task completion before deadlines. The resulting challenge is to design fair and efficient distributed resource scheduling mechanisms that jointly serve HUs and MUs while ensuring stable operation and provable convergence guarantees.

The above four challenges form the motivation of our work. Specifically, to address them, we develop a forecasting-driven agent scheduling and incentive optimization (FUSION) framework for distributed service provisioning. In FUSION, to address challenge (A), we design a proactive spatio-temporal demand prediction via liquid neural networks (*Pro-LNN*), which transforms historical service traces and contextual features into multi-step workload forecasts. Then, to address challenge (B), we propose an enhanced ant colony optimization for vehicular route planning (*eACO-VRP*) based on the predicted demand. Afterwards, to address challenge (C), we introduce offline auction-based incentive-compatible contracting (*Off-AIC²*) that matches ESs with proper APs and obtains payments and rewards. Finally, to address challenge (D), we formulate an efficient online potential game among HUs, MUs, and ES/UAV, and propose the potential game-based best-response dynamics (*PG-BRD*) method, which integrates potential-guided dual decomposition with asynchronous best-response dynamics to drive the system towards a pure-strategy Nash equilibrium (NE) under congestion and fairness constraints. To sum up, our major contributions can be summarized as follows:

- We present one of the first air-ground integrated edge network models that jointly captures vehicular-UAV APs, ESs, and heterogeneous human-machine (i.e., HU-MU) computing demands within a single framework.
- We formulate ES-AP-user service provisioning by accounting for spatio-temporal mobility constraints, stochastic workload evolution, and strategic agent behaviors. We unveil that the offline ES-AP contract design admits a combinatorial mixed-integer formulation, while the online interactions between service demanders (HUs and MUs) and providers (ESs and APs) leads to a finite ordinal

potential game with a combinatorial action space. To tackle these formulations, we develop a two-stage solution consisting of a forecast-driven offline stage and a game-theoretic online stage.

- For the offline stage, we develop a multi-step spatio-temporal demand forecasting framework via *Pro-LNN* with executable vehicle-UAV route planning through an enhanced ACO-based algorithm (i.e., *eACO-VRP*). To our knowledge, this represents one of the first applications of the emerging LNN paradigm to spatio-temporal workload forecasting for proactive decision-making in air-ground integrated networks.
- To address forecast-driven risk and strategic interactions in the offline stage, we propose *Off-AIC²*, a novel auction-based offline ES-AP contracting mechanism that incorporates demand forecasts into demand-supply matching and resource pricing, with provable guarantees of individual rationality, incentive compatibility, and budget feasibility.
- For the online stage, we model real-time task scheduling as a multi-player potential game involving HUs, MUs, and heterogeneous ES/UAV resources. We then design *PG-BRD*, a potential-guided best-response algorithm with convergence guarantees to a pure-strategy NE.
- Through extensive evaluations, we show that FUSION consistently delivers higher social welfare while keeping the delay and energy costs on par with existing baselines.

2 RELATED WORK

2.1 Service Provision in UAV-Assisted Edge Networks

There exist an extensive literature on improving the communication/computation performance and reducing the energy footprint of UAV-assisted edge computing systems [6]–[9]. For instance, Wang *et al.* [6] designed a multi-agent deep reinforcement learning (DRL)-based resource scheduling scheme for UAV-assisted wireless edge networks; Xu *et al.* [7] studied minimizing the average inference delay over UAV-assisted computing systems via DRL-based resource allocation; Li *et al.* [8] investigated distributed/federated edge intelligence for UAV-assisted networks, while optimizing the UAV energy consumption and resource utilization; Zeng *et al.* [9] introduced an ES-assisted UAV navigation system that integrates DRL-based decision making with network-aware containerized resource allocation to maximize the quality of navigation.

Although the above studies offer valuable insights, they predominantly presume that UAVs are always *nearby and can provide immediate service*, often without explicitly modeling their underlying deployment units or origins. As a result, the joint treatment of the four challenges summarized in Sec. 1 remains largely unexplored, an effort undertaken in this work.

2.2 Auction-Driven and Game-Theoretic Service Provisioning

Auctions have been widely used for resource provisioning from service providers to users. For instance, Ren *et al.* [15] investigated truthful auctions for dependent task scheduling over dynamic edge networks; Xu *et al.* [16] designed combinatorial auction-based deep neural network (DNN) inference for heterogeneous edge-cloud networks to maximize social welfare; Li *et al.* [17] developed an online auction for generative content scheduling; Lu *et al.* [18] proposed auction-based distributed/federated learning to

TABLE 1
A summary of related studies
(ST: Spatio-Temporal, Pred.: Predictive, Het.: Heterogeneous)

Reference	Network Characteristics			Service Delivery			Participant	
	Static	Dynamic	ST	Offline	Online	Pred.	Het. users	Het. ESs
[6]		✓	✓		✓			
[7]		✓			✓		✓	
[8]		✓		✓				✓
[9]		✓			✓			
[12], [19], [20]	✓			✓				✓
[13]	✓			✓				✓
[15]		✓	✓	✓			✓	✓
[16], [17]		✓			✓		✓	✓
[18]		✓		✓			✓	
This Work		✓	✓	✓	✓	✓	✓	✓

improve the distributed model training speed and energy consumption in edge networks. While the above studies provide valuable insights, they are mostly *reactive* (i.e., decisions are made after demand realization), and typically assume fixed resources and stable demand. In contrast, UAV-assisted edge computing involves dynamic resources and stringent delay and energy constraints, calling for spatio-temporally-aware auctions with minimal online interactions between service providers and end users while accounting for uncertainties in both resource availability and demand. This gap is addressed by our Off-AIC² framework.

Beyond auctions, potential games have also been explored as distributed optimization strategies for service provisioning [12], [13]. For example, *Ding et al.* [12] investigated task processing across user–edge–cloud networks as potential games; *Zhou et al.* [13] modeled computation offloading as a potential game with latency–energy trade-offs; *Hsieh et al.* [19] proposed a knapsack potential game for task scheduling; *Wu et al.* [20] studied task scheduling for multi-cell edge–cloud networks through potential games with NE guarantees. Despite their notable contributions, the above works typically consider a single/homogeneous user type, overlooking the fundamentally different QoS requirements of HUs and MUs, as well as their interactions with heterogeneous ESs. Consequently, the effectiveness of potential games in UAV-assisted platforms that support human-machine coexistence, spatio-temporal task windows, and multi-party interactions remains largely unexplored, an effort addressed via our developed PG-BRD.

To further highlight our contributions, Table 1 compares our approach with representative existing studies.

3 OVERVIEW AND MODELING

3.1 Overview of Our Methodology

We consider an air-ground integrated network, wherein nodes are partitioned into *service demanders* and *service providers*.

1) *Service demanders (SDs)*: SDs are users that generate tasks such as model training/inference¹. To capture different QoS needs under human-machine coexistence, we further classify SDs into two categories:

- **HUs**, denoted by $\mathcal{U}^H = \{u_1^H, \dots, u_{|\mathcal{U}^H}|^H}\}$ are sensitive to instantaneous service latency, as applications such as AR/VR, interactive gaming, real-time video conferencing,

1. We assume that each SD is associated with one task that requires computing services from SPs in every future trading round.

and intelligent driving are interactive and experience-driven, where even a slight change in latency or QoS can leave a pronounced impact on their perceived utility.

- **MUs**, denoted by $\mathcal{U}^M = \{u_1^M, \dots, u_{|\mathcal{U}^M}|^M}\}$, correspond to autonomous devices such as robots, mapping vehicles, and sensing units. MUs are primarily concerned about whether their computation tasks can be completed before a certain deadline, and are therefore less impacted by instantaneous latency, as long as their overall task feasibility is preserved (e.g., a robot’s image-analysis task is considered feasible as long as the inference results are obtained before the deadline).

2) *Service providers (SPs)*: We consider two types of SPs:

- **ESs**, denoted by $\mathcal{S} = \{s_1, \dots, s_{|\mathcal{S}|}\}$, are geo-distributed across the map and provide low-latency services to nearby users. Each ES operates with a limited pool of orthogonal subcarriers and finite resource capacity, inherently constraining the number of users that can be concurrently served. During peak demand periods, hotspot ESs are particularly susceptible to resource saturation, which can trigger substantial queuing delays or even admission blocking.
- **APs**, denoted by $\mathcal{V} = \{v_1, \dots, v_{|\mathcal{V}|}\}$, are formed by vehicles carrying multiple on-board charging UAVs. Due to the limited power of UAVs, vehicles first traverse pre-planned routes to transport UAVs to designated service/ES locations. Upon arriving at their contracted ESs, UAVs are deployed to offer extra computing resources. This procedure incurs operational costs, including vehicle repositioning, UAV dispatching/launching procedures, flight energy consumption, and maintenance overhead.

Under this two-sided demand-supply structure, SDs compete for reliable computing services, while SPs collaboratively offer computing resources under their capacity and operational limitations. Nevertheless, in such a dynamic and distributed ecosystem, ESs face *uncertain service demand*: the temporal and spatial distribution of service request peaks across ESs is highly stochastic, and the composition ratio between HUs and MUs in the service requests also varies over time. To capture the time-varying behavior, a practical transaction is discretized into T time-slots, with index t , i.e., $t \in \{0, 1, 2, \dots, T\}$. Further, to enable resource provisioning between SDs and SPs, we adopt a two-stage resource allocation framework that explicitly separates an offline stage from an online stage. From the ES perspective, the offline stage operates before the actual trading round, when only historical records and statistical demand patterns are available. At this stage (detailed in Sec. 4), the identities and tasks of HUs and MUs in the next trading round are unknown, making it impossible to pre-plan precise AP-ES matchings. Accordingly, in the offline stage of Fig. 1, we train Pro-LNN to forecast future service demand for each ES, and, based on these predictions, jointly design AP-to-ES visiting routes, UAV deployment plans, and auction-based contracts between ESs and APs (i.e., Off-AIC²).

In contrast, the online stage starts (detailed in Sec. 5) when real computing tasks arrive and the actual identities and locations of SDs become known. With full knowledge of active participants and their instantaneous task requirements, the system performs real-time task–resource scheduling. In this stage, we model the interactions among heterogeneous SPs and SDs as a potential game and construct an *ordinal*

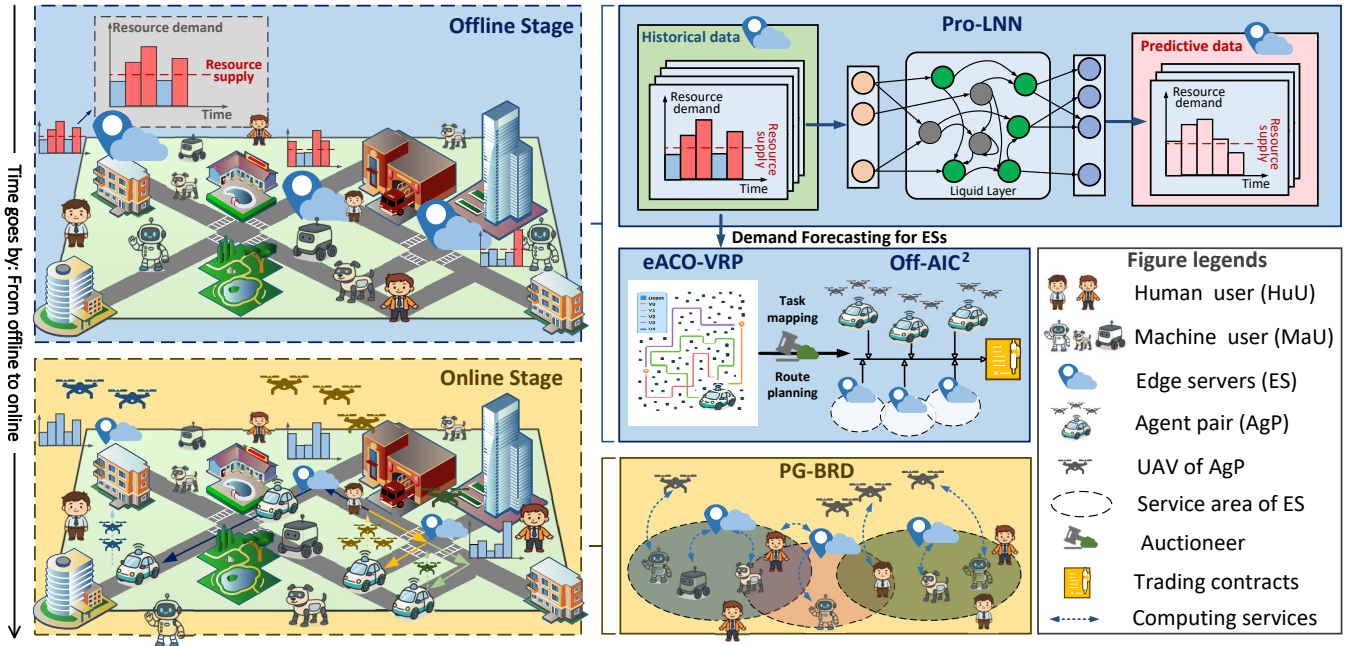


Fig. 1. Schematic of FUSION over an air-ground integrated network.

potential that captures the social welfare. Each SD then updates its task offloading decision and each SP adjusts its service admission in a *fully distributed* manner, where the resulting potential-guided best-response dynamics converge to a pure-strategy NE, yielding an online and congestion-aware provisioning of resources.

3.2 Modeling of SDs, SPs, and Contracts

Hereafter, we provide detailed modeling of SPs and SDs.

3.2.1 Modeling of SDs

We model HUs and MUs as follows:

(i) **HUs:** Each HU $u_m^H \in \mathcal{U}^H$ is modeled by a 5-tuple $u_m^H = \{e_m^{H,tx}, r_m^H, d_m^H, f_m^{H,loc}, C_m^H\}$, where $e_m^{H,tx}$ is its up-link transmit power (Watts); r_m^H is its required computing workload (CPU cycles); d_m^H is its input data size (bits); $f_m^{H,loc}$ is its local CPU frequency; and C_m^H represents the set of reachable ESs within the communication coverage of u_m^H .

(ii) **MUs:** Each MU $u_n^M \in \mathcal{U}^M$ is represented by a 6-tuple $u_n^M = \{\tau_n^{ddl}, e_n^{M,tx}, r_n^M, d_n^M, f_n^{M,loc}, C_n^M\}$, where τ_n^{ddl} is its task deadline time; $e_n^{M,tx}$ is its transmit power; r_n^M and d_n^M denote its workload and data size, respectively. Also, $f_n^{M,loc}$ denotes its CPU capability, and C_n^M captures SPs that can serve u_n^M .

3.2.2 Modeling of SPs

We model ESs and APs as follows:

(i) **ESs:** Each ES $s_i \in \mathcal{S}$ is represented by a 6-tuple: $s_i = \{t_i^{E,b}, f_i^E, e_i^E, G_i, l_i^{E,b}\}$, where $t_i^{E,b}$ denotes the time-slot at which s_i begins to request resource supply to mitigate the shortage of edge resources within its own coverage area; f_i^E is its computing capacity (e.g., CPU cycles/s); e_i^E is its local power consumption (Watts); $l_i^E = (x_i^E, y_i^E, h_i^E)$ is its 3D location. In addition, each ES s_i is presumed to have a set of orthogonal subcarriers that can serve at most G_i SDs simultaneously.

(ii) **APs:** each AP $v_k \in \mathcal{V}$ is modeled by a 7-tuple: $v_k = \{C_k^A, f_k^A, e_k^{comp}, e_k^{move}, e_k^{fly}, G_k^A, l_k^A\}$, where C_k^A denotes the maximum number of UAVs carried by the vehicle;

f_k^A captures the computing capability of each mounted UAV; e_k^{move} , e_k^{comp} , and e_k^{fly} denote the power consumption of ground movement, UAV computation, and UAV flight, respectively; G_k^A denotes the maximum number of SDs that each UAV of v_k can serve through its limited orthogonal subcarriers; $l_k^A(t) = (x_k^A(t), y_k^A(t))$ is the ground location of the vehicle at time t .

3.2.3 Modeling of Offline Contracts

In the offline stage, a trading contract is established between each ES s_i and AP v_k , denoted as $C_{i,k}^{E \leftrightarrow A} = \{N_{i,k}^{Trad}, p_{i,k}^{ES}, r_{i,k}^{ES}\}$, where $N_{i,k}^{Trad}$ represents the quantity of traded resources, $p_{i,k}^{ES}$ indicates unit payment (per task) from s_i to contractual AP v_k , and $r_{i,k}^{ES}$ refers to the unit reward (per task) of v_k for offering services.

4 OFFLINE STAGE: FORECASTING-DRIVEN CONTRACTING AND AP DEPLOYMENT

We first delve into capturing the service leasing among different types of SPs, for which we systematically transform the handling of uncertain spatio-temporal service demand into proactive, incentive-compatible, and cost-aware AP deployment decisions. Our major efforts include: (i) a predictive workload forecasting module that estimates the spatiotemporal dynamics of demands across distributed ESs; (ii) a cost-aware vehicle routing strategy based on eACO, which constructs time-window-feasible candidate associations/matching of APs to ESs; (iii) a contract-design module that leverages an incentive-compatible auction mechanism to determine long-term cooperative agreements between ESs and APs, including winning trading pairs, allocated tasks, and corresponding payment rules.

We let $x_{i,k}^{Off}$ denote the assignment/matching between ESs and APs, where $x_{i,k}^{Off} = 1$ indicates that ES s_i successfully secures the service of AP v_k and thereby signs an offline contract, and $x_{i,k}^{Off} = 0$ otherwise. For notational simplicity, we define $\mathbf{X}^{Off} = \{x_{i,k}^{Off} \mid s_i \in \mathcal{S}, v_k \in \mathcal{V}\}$ as the assignment profile.

4.1 Utilities of ESs, AP, and Auctioneer

4.1.1 Utility of ESs

In the offline stage, as delivering edge services to users and leasing computing capacity can generate both costs and revenues for ESs, we model the utility of each ES s_i as its net profit as follows:

$$U_i^{\text{ES,Off}} = \sum_{v_k \in \mathcal{V}} x_{i,k}^{\text{Off}} N_{i,k}^{\text{Trad}} \left(\bar{p}_i - p_{i,k}^{\text{ES}} \right), \quad (1)$$

where \bar{p}_i denotes the historical average payment earned by s_i for providing edge services to users.

4.1.2 Utility of APs

We model the utility of each AP as a combination of four key components: (i) *Vehicular moving cost*: the energy cost incurred by the vehicle traveling to ES s_i is given by: $c_{i,k}^{\text{move}} = \tau_{i,k}^{\text{move}} e_k^{\text{move}}$, where $\tau_{i,k}^{\text{move}}$ denotes the traveling time of the carrier vehicle when moving from its origin to the target ES s_i , which depends on the driving distance and the AP's vehicular speed; (ii) *UAV flying cost*: the energy consumption during UAV flight is given by: $c_{i,k}^{\text{fly}} = \tau_{i,k}^{\text{fly}} e_k^{\text{fly}}$, where $\tau_{i,k}^{\text{fly}}$ denote the total UAV flight time spent shuttling between s_i and its associated service region, which increases with the number and size of the tasks to be served; (iii) *UAV computing cost*: the energy consumed by each UAV while providing resources is given by: $c_{i,k}^{\text{comp}} = \tau_{i,k}^{\text{comp}} e_k^{\text{comp}} = \frac{\bar{r} e_i^{\text{ES}}}{f_k^{\text{A}}}$, where \bar{r} denotes the historical average computational workload per task², and $\tau_{i,k}^{\text{comp}}$ represents the effective computing time that the UAV dedicates to processing offloaded tasks, determined by the aggregate computational workload and the UAV's computing capability; (iv) *Income for service provisioning*: the revenue obtained from contributing resources is denoted by $r_{i,k}^{\text{ES}}$. The overall utility of v_k can therefore be expressed as follows:

$$U_k^{\text{A,Off}} = \sum_{s_i \in \mathcal{S}} x_{i,k}^{\text{Off}} \omega_1 \left(r_{i,k}^{\text{ES}} - c_{i,k}^{\text{move}} - c_{i,k}^{\text{fly}} - N_{i,k}^{\text{Trad}} c_{i,k}^{\text{comp}} \right) + \omega_2 c^{\text{hard}}, \quad (2)$$

where ω_1 and ω_2 denote cost coefficients that convert energy consumption into monetary units (e.g., dollars), and c^{hard} represents the hardware depreciation/maintenance cost.

4.1.3 Utility of the Auctioneer

An auctioneer (e.g., a trusted third party), plays a pivotal role in coordinating interactions among APs and ESs, including bids/asks collection, determining winning APs-ESs associations, and trading contract design. We define the utility of auctioneer as the difference between the income obtained by APs and the expense paid by ESs:

$$U^{\text{Auc,Off}} = \sum_{s_i \in \mathcal{S}} \sum_{v_k \in \mathcal{V}} x_{i,k}^{\text{Off}} N_{i,k}^{\text{Trad}} \left(p_{i,k}^{\text{ES}} - r_{i,k}^{\text{ES}} \right). \quad (3)$$

4.2 Problem of Interest in Offline Stage of FUSION

Our overarching goal during the offline stage of FUSION is maximizing the social welfare (SW) defined as the collective utilities of engaged parties (i.e., ESs, APs, auctioneer) as:

$$U^{\text{SW}} = \sum_{s_i \in \mathcal{S}} U_i^{\text{ES,Off}} + \sum_{v_k \in \mathcal{V}} U_k^{\text{A}} + U^{\text{Auc}}. \quad (4)$$

During this offline stage, we determine the optimal winning ES-AP pairs (i.e., $x_{i,k}^{\text{Off}}$ combinations), while establishing their corresponding trading contracts, (i.e., determining

2. Since trading is conducted in the offline stage, APs do not know the exact sizes of the tasks they will eventually process and can only evaluate them based on historical average data.

$\mathbb{C}_{i,k}^{\text{E} \leftrightarrow \text{V}}$), formulated by an optimization problem $\mathcal{F}^{(1)}$ as follows:

$$\mathcal{F}^{(1)} : \operatorname{argmax}_{x_{i,k}^{\text{Off}}, \mathbb{C}_{i,k}^{\text{E} \leftrightarrow \text{V}}} U^{\text{SW}} \quad (5)$$

$$\text{s.t.} \quad \sum_{v_k \in \mathcal{V}} x_{i,k}^{\text{Off}} \leq 1, \quad \forall s_i \in \mathcal{S} \quad (5a)$$

$$x_{i,k}^{\text{Off}} \in \{0, 1\}, \quad \forall s_i \in \mathcal{S}, \forall v_k \in \mathcal{V} \quad (5b)$$

$$\sum_{s_i \in \mathcal{S}} x_{i,k}^{\text{Off}} N_{i,k}^{\text{Trad}} \leq G_k^{\text{A}}, \quad \forall v_k \in \mathcal{V} \quad (5c)$$

where (5a) ensures that each ES is matched with (at most) an AP, (5b) enforces the binary nature of $x_{i,k}^{\text{Off}}$, and (5c) guarantees that the promised resources in signed contracts do not exceed the supply of each AP v_k . Problem $\mathcal{F}^{(1)}$ is an NP-hard mixed-integer linear programming (MILP) problem [21], [22] that involves both discrete (e.g., $x_{i,k}^{\text{Off}}$) and continuous variables (e.g., $\mathbb{C}_{i,k}^{\text{E} \leftrightarrow \text{V}}$). To tackle this problem, we first note that the quality of any auction-based solution fundamentally depends on how accurately the future resource usage can be predicted. Motivated by this, in the following, we first develop Pro-LNN to estimate the spatio-temporal demands of ESs; then, based on these forecasts, we design eACO-VRP to plan APs' service routes and recommend suitable ES sets. Building on these two components, we finally design the Off-AIC² that determines the winning ES-AP association pairs together with their contracts.

4.3 Forecasting, Agent Deployment, and Contracting

We next present the offline stage that couples demand forecasting, AP deployment, and long-term contracting. The overall interaction flow of the proposed Pro-LNN + eACO-VRP + Off-AIC² framework as follow:

- At the beginning of each offline trading round, each ES locally runs Pro-LNN to predict its service demand over future rounds, and submits the resulting demand profile as bid information to the auction platform. Each AP, in turn, reports its available service capacity and ask price based on its computing capability, energy consumption, and available service duration.
- After collecting all bids and asks, the auction platform first invokes Off-AIC² to filter out infeasible ES-AP pairs under price and capacity constraints, and then calls eACO-VRP³ on the resulting candidate set to determine, for each winning AP, the set of ESs to be served and their visiting order, thereby generating pre-planned routes that jointly account for time windows, travel distance, and utility.
- Subsequently, Off-AIC² applies its critical-price-based pricing rules to compute settlement payments for winning ESs and rewards for winning APs.
- The final offline outcome includes the ES-AP matching relations, the payment vectors, and the pre-planned service routes for each AP, which will be taken as inputs to the online stage over the subsequent time horizon.

In what follows, we describe the three modules, i.e., Pro-LNN-based demand forecasting, eACO-VRP-based AP deployment, and the Off-AIC² contracting mechanism.

3. Note that eACO-VRP serves as a route-aware matching subroutine inside Off-AIC², and the two methods are tightly coupled in the actual mechanism. For clarity of exposition, however, we present the standalone design of eACO-VRP before introducing the complete Off-AIC² procedure later in this subsection.

4.3.1 Design of Proactive Spatio-Temporal Demand Prediction via Liquid Neural Networks (Pro-LNN)

Unlike discrete-time recurrent neural networks (RNNs) or Transformers, LNNs [23] implement continuous-time dynamics with neuron-wise time constants and exponential-style state updates. This makes them particularly suitable for modeling time series that are sampled at irregular resource trading intervals, exhibit non-stationary spatio-temporal demand patterns, and must be processed under strict edge-computing resource constraints. In our setting, Pro-LNN takes as input the ES-side demand time series across trading rounds $\nu = 1, 2, \dots$, where the time gaps $\Delta\nu$ between rounds can be irregular and some observations may be missing due to asynchronous reporting. The predictor therefore must stay stable under such irregular $\Delta\nu$ while capturing both short-term and long-term trends, motivating our LNN-based architecture.

Let $N_i^{\text{Dem},(\nu)}$ denote the task demand of ES s_i at the ν -th trading round. We form an input vector $\mathbf{z}_i^{(\nu)} = [N_i^{\text{Dem},(\nu)}, \mathbf{x}_i^{(\nu)}]$, where $\mathbf{x}_i^{(\nu)}$ stacks optional exogenous features at round ν , such as time-of-day and day-of-week indicators, ES-type and capacity descriptors, and local mobility/load statistics extracted from recent logs. Given a length- L history of past observations $\{\mathbf{z}_i^{(\nu-L+1)}, \dots, \mathbf{z}_i^{(\nu)}\}$, Pro-LNN encodes this sequence via a liquid cell with neuron-wise time constants, integrates the measurements into a hidden state $\mathbf{h}_i^{(\nu)}$, and then applies a shallow readout network to produce an H -step forecast $\{\hat{N}_i^{\text{Dem},(\nu+1)}, \dots, \hat{N}_i^{\text{Dem},(\nu+H)}\}$. In a nutshell, Pro-LNN is trained with a composite loss, which is an H -step MSE between the forecasts and the ground-truth demands, and we additionally use a multi-step consistency regularizer that rolls the predictor forward in closed-loop over H steps and penalizes the accumulated prediction errors at future trading rounds. These forecasts are computed offline before each trading round and then fed into the eACO-VRP module for ES recommendation and AP route pre-planning, as well as the auction module for ES-AP contract design. The detailed update equations and training pseudocode of our Pro-LNN are deferred to Appx. B.1 to avoid detracting from the main discussion.

4.3.2 Enhanced Ant Colony Optimization for Vehicle Route Planning (eACO-VRP)

Within the proposed offline stage of FUSION, once Off-AIC² has identified a feasible trading region and candidate ES-AP pairs, the auction platform still needs to decide, for each winning AP, which ESs should be physically visited and in what order, under time-window and capacity constraints. This induces a capacitated vehicle-routing problem with time windows and heterogeneous travel costs and utilities. Since our APs (e.g., UAVs or service vehicles) and the auction platform operate under tight energy and latency budgets and should periodically recompute routes as demand forecasts change, we adopt a lightweight ant colony optimization (ACO) paradigm and tailor it into an eACO-VRP that can be invoked as a subroutine inside Off-AIC², balancing solution quality with low computational complexity and energy cost.

Inspired by ACO [25], [26] and tailored to the heterogeneity of ESs (e.g., distinct time windows and locations) and APs (e.g., diverse costs), we develop the eACO-VRP, which makes each AP select a set of ESs and a pre-planned service route (i.e., an ES visiting sequence) to maximize

its utility. For a given v_k , we model v_k and all ESs as vertices of a directed complete graph $\mathcal{G}_k(\mathcal{N}_k, \mathcal{E}_k)$. Here, $\mathcal{N}_k = \{n_0, n_1, \dots, n_{|\mathcal{S}|}\}$ denotes the vertex set, where n_0 represents v_k and $n_1, \dots, n_{|\mathcal{S}|}$ denote ESs; while the edge set is $\mathcal{E}_k = \{(n_r, n_s) \mid n_r, n_s \in \mathcal{N}_k, r \neq s\}$. Let the initial location of n_0 be $l_0^v \langle 0 \rangle$, and the fixed locations of $n_1, \dots, n_{|\mathcal{S}|}$ be $l_1^s, \dots, l_{|\mathcal{S}|}^s$. We use \mathbb{K} to denote the set of ants: each ant $\mathbb{k} \in \mathbb{K}$ simulates the trajectory of v_k , starting from $l_0^v \langle 0 \rangle$. At each step, it evaluates: the current time-slot, the starting time-slot when ES s_i begins to request extra resources, the travel time to each candidate ES, and the utility upon arrival; it then selects a feasible next vertex to visit (i.e., a vertex whose arrival time, computed as the current time plus travel time, precedes the starting time-slot at which the candidate ES begins requesting extra resource supply). The state-transition rule, i.e., the probability that ant \mathbb{k} moves from n_r to n_s ($r \neq s \neq 0$) is

$$pr_{r,s}^{\mathbb{k}} = \begin{cases} \frac{\varphi_{r,s}^{\varepsilon_1} \eta_{r,s}^{\varepsilon_2} (1/\text{width}_s)^{\varepsilon_3}}{\sum_{q \in J^{\mathbb{k}}(n_r)} \varphi_{r,q}^{\varepsilon_1} \eta_{r,q}^{\varepsilon_2} (1/\text{width}_q)^{\varepsilon_3}} & \text{if } n_s \in J^{\mathbb{k}}(n_r), \\ 0 & \text{otherwise,} \end{cases} \quad (6)$$

with positive weights $\varepsilon_1, \varepsilon_2, \varepsilon_3$. In (6), $\varphi_{r,s}$ denotes the pheromone level on edge (n_r, n_s) (see (7)); $\eta_{r,s}$ is the distance between n_r and n_s . If the ant arrives early (i.e., before the time-slot when ES s_i begins to request extra resources), it can pre-position the AP's UAV at this ES; in this case, the remaining time width_s is defined as the difference between the arrival time and the time-slot when ES s_i begins to request extra resources. Conversely, if the ant reaches n_s after the time-slot when ES s_i begins to request extra resources, this ES is regarded as infeasible and eliminated in the route construction. In (6), $J^{\mathbb{k}}(n_r)$ denotes the set of feasible ES vertices that ant \mathbb{k} can reach when standing at node n_r : an ES $n_s \in J^{\mathbb{k}}(n_r)$ if it satisfies two feasibility conditions: (i) the current time plus the travel time from n_r to n_s should not exceed the time-slot when ES s_i begins to request extra resources, and (ii) there must still be remaining UAVs at AP v_k to deploy. Once a route is found by ants, pheromones on edges are updated as follows:

$$\varphi_{r,s} \leftarrow (1 - \theta) \varphi_{r,s} + \Delta\varphi_{r,s}, \quad (7)$$

where $0 < \theta < 1$ is the evaporation coefficient, and

$$\Delta\varphi_{r,s} = \begin{cases} \sum_{(n_r, n_s) \in M^{\max}} \Delta U_{r,s}^A, & \text{if } (n_r, n_s) \in M^{\max}, \\ 0, & \text{otherwise,} \end{cases} \quad (8)$$

captures the deposited pheromone, where $\Delta U_{r,s}^A$ denotes the utility increment for v_k when moving from n_r to serve the ES at n_s , and $M^{\max} = \{M^{\mathbb{k}} \mid \max \sum_{(r,s) \in M^{\mathbb{k}}} \Delta U_{r,s}^A, \forall \mathbb{k} \in \mathbb{K}\}$ denotes the path with the largest utility among ants. For brevity, the pseudo-code of eACO-VRP is provided in Alg. 1, while its four main steps are summarized below:

Step 1. Initialization (lines 1-2, Alg. 1): Using the AP/ES information (e.g., geographic locations, the time-slot when ES s_i begins to request extra resources, AP v_k payments and service costs, and the travel/service time and energy), we construct, for each AP v_k (with source node n_0), a graph $\mathcal{G}_k(\mathcal{N}_k, \mathcal{E}_k)$ as discussed above.

Step 2. Path exploration (lines 4-13, Alg. 1): At each iteration, an ant \mathbb{k} located at its current vertex n_r jointly evaluates the current time-slot, the travel time to each vertex, the

Algorithm 1: Proposed eACO-VRP

```

1 Input: AP  $v_k$  (source node  $n_0$ ), ES set  $\mathcal{S}$ , directed complete graph
    $\mathcal{G}_k(\mathcal{N}_k, \mathcal{E}_k)$ , ant set  $\mathbb{K}$ , max iterations  $iter_{max}$ 
2 Initialization:  $\varphi_{r,s} \leftarrow \varphi_0$  for all  $(n_r, n_s) \in \mathcal{E}_k$ ;  $iter \leftarrow 1$ 
3 while  $iter \leq iter_{max}$  do
4   for each ant  $k \in \mathbb{K}$  do
5      $M^k \leftarrow \emptyset$ ;  $n_r \leftarrow n_0$ 
6     while end condition not met do
7       Compute: feasible set  $J^k(n_r)$  and transition probabilities
          $p_{r,s}^k$  (via (6))
8       if  $J^k(n_r) \neq \emptyset$  then
9         sample next node  $n_s$  according to  $p_{r,s}^k$  from  $J^k(n_r)$ 
10         $M^k \leftarrow M^k \cup \{\text{edge}(n_r, n_s)\}$ 
11         $n_r \leftarrow n_s$ 
12      else
13        break
14     $M^{max} \leftarrow \arg \max_{M^k: k \in \mathbb{K}} \sum_{(n_r, n_s) \in M^k} \Delta U_{r,s}^W$ 
15    for each  $(n_r, n_s) \in \mathcal{E}_k$  do
16      Pheromone evaporation and deposit (7) and (8)
17     $iter \leftarrow iter + 1$ 
18 Output:  $M^{max}$  (pre-planned route for  $v_k$ ), and the recommended ES
    tasks along  $M^{max}$ 

```

service time at that vertex, and the time-slot when ES s_i begins to request extra resources. This screening step yields the feasible candidate set $J^k(n_r)$ and the associated transition probabilities $p_{r,s}^k$ as discussed above. The ant then probabilistically selects its next vertex using (6).

Step 3. Pheromone update (lines 14-16, Alg. 1): For each constructed path M^k , we compute the cumulative utility $\sum_{(r,s) \in M^k} \Delta U_{r,s}^A$. Among all ants, the path with the largest utility is selected as M^{max} , and the pheromone trails on its edges are reinforced according to (7) and (8), while pheromones on other edges evaporate.

Step 4. Output (line 18, Alg. 1): After finishing all the iterations, the route M^{max} with the highest utility is returned as the pre-planned path for AP v_k , and the ES tasks located along this route are recommended as its preferred service targets.

4.3.3 Offline Auction-based Incentive-Compatible Contracting (Off-AIC²)

Building on the pre-planned AP routes obtained above, we now introduce Off-AIC², an offline double-auction mechanism that establishes incentive-aware service contracts between ESs and APs. The goal is to decide ES-AP associations, how much service capacity should be reserved along each AP route, and how payments/rewards should be set so that participants (i.e., ESs and APs) have limited incentive to misreport their private values.

In Off-AIC², on the *buyer* side, each ES s_i predicts its total service demand N_i^{Dem} (e.g., the number of service units or tasks that need to be supported in the next trading round) and has a private per-unit valuation v_i for receiving edge service. It then participates in Off-AIC² by submitting a per-unit bid bid_i together with its demand N_i^{Dem} , where bid_i represents the maximum payment it is willing to make per unit of service. On the *seller* side, each AP v_k , based on its maximum service capacity C_k^A (e.g., the total number of service units it can provide) and its service cost, reports a per-unit ask price ask_k and its capacity C_k^A , where ask_k is the minimum acceptable payment per unit of service. Subsequently, for a potential ES-AP pair (s_i, v_k) , we define a pairwise utility

Algorithm 2: Proposed Off-AIC²

```

1 Input: ES set  $\mathcal{S}$  with demands  $\{N_i^{\text{Dem}}\}$  and per-ES bids  $\{\text{bid}_i\}$ ; AP set
    $\mathcal{V}$  with asks  $\{\text{ask}_k\}$  and capacities  $\{C_k^A\}$ 
2 Initialization: Set  $\mathbf{X}^* \leftarrow \mathbf{0}$ ,  $\mathbf{p}^{b*} \leftarrow \mathbf{0}$ ,  $\mathbf{r}^{s*} \leftarrow \mathbf{0}$ .
3 Sort ES indices into  $\mathcal{L}^{\text{ES}}$  by  $\text{bid}_i$  (descending), and AP indices into  $\mathcal{L}^{\text{AP}}$ 
   by  $\text{ask}_k$  (ascending); relabel  $(i, k)$  accordingly.
4 Find a pair of pivotal ranks  $(I^*, K^*)$  such that
    $\text{bid}_{I^*} \geq \text{ask}_{K^*}$ ,  $\sum_{k=1}^{K^*} C_k^A \geq \sum_{i=1}^{I^*} N_i^{\text{Dem}}$ , and  $I^*$  is
   maximized (breaking ties by larger capacity slack
    $\sum_{k=1}^{K^*} C_k^A - \sum_{i=1}^{I^*} N_i^{\text{Dem}}$ ).
5 Initialize the set of unmatched ESs:  $\mathcal{U}^{\text{free}} \leftarrow \{s_i \mid 1 \leq i \leq I^*\}$ .
6 for  $k$  in top- $K^*$  APs (according to  $\mathcal{L}^{\text{AP}}$ ) do
7   if  $C_k^A \leq 0$  or  $\mathcal{U}^{\text{free}} = \emptyset$  then
8     continue
9   Build candidate ES set
     $\mathcal{C}_k \leftarrow \{s_i \in \mathcal{U}^{\text{free}} \mid U_{i,k}^{\text{Off}} > 0 \wedge \text{bid}_i \geq \text{ask}_k\}$ ;
10  if  $\mathcal{C}_k = \emptyset$  then
11    continue
12   $\mathcal{K}_k^* \leftarrow \text{Alg. 2}$ ;
13  for  $i \in \mathcal{K}_k^*$  do
14    Set  $x_{i,k}^{\text{Off}} \leftarrow 1$ ;
15    Remove  $s_i$  from  $\mathcal{U}^{\text{free}}$ :  $\mathcal{U}^{\text{free}} \leftarrow \mathcal{U}^{\text{free}} \setminus \{s_i\}$ ;
16  Update remaining capacity:  $C_k^A \leftarrow C_k^A - \sum_{i \in \mathcal{K}_k^*} N_i^{\text{Dem}}$ .
17 Denote the resulting matching by  $\mathbf{X}^* = \{x_{i,k}^{\text{Off}}\}$ .
18 for each matched ES  $s_i$  with  $\sum_k x_{i,k}^{\text{Off}} = 1$  do
19   Set  $high \leftarrow \text{bid}_i$ ,  $low \leftarrow \text{bid}_{I^*+1}$ ;
20   while  $low < high$  do
21     Set  $b_{\text{eff}} \leftarrow (low + high)/2$ ;
22     Rerun Step 2 on the top- $I^*$  ESs and top- $K^*$  APs, using  $b_{\text{eff}}$  as
     ES  $s_i$ 's bid and keeping all other bids/asks unchanged, to
     obtain a temporary matching  $\mathbf{X}^{\text{Temp}}$ ;
23     if  $\sum_k x_{i,k}^{\text{Temp}} = 1$  then  $high \leftarrow b_{\text{eff}}$ ;
24     else  $low \leftarrow b_{\text{eff}}$ ;
25   Set  $p_i^{b*} \leftarrow high$ .
26 for each matched AP  $v_k$  with  $\sum_{s_i} x_{i,k}^{\text{Off}} \geq 1$  do
27   Set  $high \leftarrow \text{ask}_k$ ,  $low \leftarrow \text{ask}_{K^*+1}$  (or a safe reserve);
28   while  $low < high$  do
29     Set  $\text{ask}_{\text{eff}} \leftarrow (low + high)/2$ ;
30     Rerun Step 2 on the top- $I^*$  ESs and top- $K^*$  APs, using  $\text{ask}_{\text{eff}}$ 
     as AP  $k$ 's ask (and keeping all other bids/asks unchanged), to
     obtain a temporary matching  $\mathbf{X}^{\text{Temp}}$ ;
31     if  $\sum_{s_i} x_{i,k}^{\text{Temp}} \geq 1$  then  $low \leftarrow \text{ask}_{\text{eff}}$ ;
32     else  $high \leftarrow \text{ask}_{\text{eff}}$ ;
33   Set  $r_k^{s*} \leftarrow low$ .
34 Output: Matching  $\mathbf{X}^*$ , ES payments  $\mathbf{p}^{b*}$ , AP rewards  $\mathbf{r}^{s*}$ .

```

$U_{i,k}^{\text{Off}} = \text{bid}_{i,k} - \text{ask}_k$ ($U_{i,k}^{\text{Off}} > 0$ indicates a socially beneficial match). Off-AIC² then uses the reported bids, asks, demands, and capacities to compute pairwise utilities and select a set of winning ESs and APs, determine their matching/association pattern, and compute payments and rewards. The complete pseudo-code of Off-AIC² is provided in Alg. 2, while its main three steps are summarized below:

Step 1. List generation and pivotal-index search (lines 3-5, Alg. 2): Off-AIC² operates as a one-shot sealed-bid double auction: all ES buyers s_i and AP sellers v_k simultaneously submit their bids, asks, and resource quantity information to an auctioneer without observing each others' submissions. We first sort ESs into a list \mathcal{L}^{ES} in descending order of bid_i , and APs into a list \mathcal{L}^{AP} in ascending order of ask_k . Without loss of generality, we relabel indices so that these sorted orders are directly reflected by i and k . The algorithm then searches for a pair of *pivotal ranks* (I^*, K^*) such that $\text{bid}_{I^*} \geq \text{ask}_{K^*}$, $\sum_{k=1}^{K^*} C_k^A \geq \sum_{i=1}^{I^*} N_i^{\text{Dem}}$.

In words, (I^*, K^*) is the largest prefix of high-bidding ESs and low-asking APs whose aggregate demand and supply can be satisfied at a non-loss-making price level.

Step 2. ES–AP matching and route planning via eACO-VRP (lines 6-16, Alg. 2): Given the pivotal ranks (I^*, K^*) , the top- I^* ESs and top- K^* APs participate in the matching stage. We initialize the set of currently unmatched ESs as $\mathcal{U}^{\text{free}} = \{1, \dots, I^*\}$ and iterate over AP sellers v_k following the order in \mathcal{L}^{AP} . For each AP v_k with remaining capacity $C_k^A > 0$ and $\mathcal{U}^{\text{free}} \neq \emptyset$, we construct a candidate ES set $\mathcal{C}_k = \{s_i \in \mathcal{U}^{\text{free}} \mid U_{i,k}^{\text{off}} > 0, \overline{\text{bid}}_i \geq \text{ask}_k\}$, where $U_{i,k}^{\text{off}} > 0$ ensures that serving s_i along some route of v_k improves the system-level SW, and $\overline{\text{bid}}_i \geq \text{ask}_k$ guarantees that the ES's per-unit value is larger than the AP's ask price.

For such an AP v_k , we invoke the eACO-VRP routine (Sec. 4.3.2), which considers ES demand volumes over time, travel time and energy cost of APs, and the payment that v_k can receive, in order to jointly determine: (i) which ESs in \mathcal{C}_k should be served without exceeding v_k 's remaining capacity C_k^A , and (ii) in what visiting order these ESs are arranged along the route of v_k . By maximizing the AP's utility over all such candidate routes, we obtain a selected ES set $\mathcal{K}_k^* \subseteq \mathcal{C}_k$ and the associated pre-planned path for AP v_k . Furthermore, for every $s_i \in \mathcal{K}_k^*$, we set $x_{i,k}^{\text{off}} = 1$ and remove s_i from $\mathcal{U}^{\text{free}}$, ensuring that each ES is matched to (at most) one AP. Stacking these per-AP decisions over all k yields the overall ES–AP assignment matrix \mathbf{X}^* . Moreover, since every successful pair (s_i, v_k) satisfies $\overline{\text{bid}}_i \geq \text{ask}_k$, each winning ES is guaranteed not to pay more than its declared value in the matching stage, which contributes to ES-side individual rationality.

Step 3. Pricing and contract finalization via binary search (lines 18-33, Alg. 2): Once \mathbf{X}^* is determined, Off-AIC² computes ES payments and AP rewards through a monotone binary-search procedure that approximates *critical-value* pricing. The high-level goal is twofold: (i) discourage large deviations from truthful bidding, and (ii) keep the total ES payment and total AP reward closely aligned so that the mechanism does not incur a systematic deficit. In particular, for each matched ES buyer s_i (with $\sum_k x_{i,k}^{\text{off}} = 1$), we treat $\overline{\text{bid}}_i$ as an *effective bid parameter* and search over the interval $[\overline{\text{bid}}_{I^*+1}, \overline{\text{bid}}_i]$ to find the smallest bid $p_i^{\text{b}*}$ such that, if s_i had declared this lower bid (while all other bids/asks remained unchanged) and Step 2 was re-executed, s_i would still be selected as a winner. This $p_i^{\text{b}*}$ is the ES's *critical payment*: bidding any lower would cause s_i to lose the contract. Symmetrically, for each matched AP seller v_k (with $\sum_i x_{i,k}^{\text{off}} \geq 1$), we vary its effective ask within $[\text{ask}_{K^*+1}, \text{ask}_k]$ and re-run Step 2 to determine the largest reward level $r_k^{\text{s}*}$ such that v_k still remains in the winning set. This $r_k^{\text{s}*}$ acts as a *critical reward*: if v_k has a higher ask, it would not be matched to any ES.

The resulting settlement vectors $(\mathbf{p}^{\text{b}*}, \mathbf{r}^{\text{s}*})$ finalize the offline contracts between ESs and APs under Off-AIC². By tying payments and rewards to these critical values, the mechanism encourages *near-truthful*⁴ reporting of private

4. Unlike conventional auctions that ignore spatio-temporal aspects of the system, truthfulness in our setting is inherently shaped by spatial advantages: ESs close to AP routes can be profitably served with lower bids, whereas remote ESs incur higher travel and time costs and must bid higher to remain competitive; similarly, APs with route-aligned demand clusters face lower marginal costs than detour-intensive ones. As ES–AP matching is jointly coupled with route planning in eACO-VRP, strict dominant-strategy truthfulness *cannot* be guaranteed. Instead, the binary-search-based payment rule approximates critical-value pricing and induces *near-truthful* behavior in practice.

valuations while keeping buyer payments and seller rewards balanced at the system level (a property that we numerically demonstrate in Sec. 6.3.3). In summary, Off-AIC² satisfies *individual rationality, approximate truthfulness, and budget balance*. Since these properties follow standard definitions, we relegate their formal definitions and detailed proofs to Appx. B.2 to maintain clarity and focus in the main text.

5 ONLINE STAGE: POTENTIAL GAMES FOR SERVICE SCHEDULING UNDER HUMAN-MACHINE COEXISTENCE

Unlike the offline stage, the online stage aims to cope with *real-time* service requests generated by HUs and MUs. In practice, the number and composition of SDs that actually arrive in each trading round may deviate from the offline forecasts. As a result, the offline outcome can only reserve a feasible pool of UAVs and service capacities for ESs with heavy resource demands, but it cannot directly determine which SP should serve which SD, at what time, or at what service rate given the real-time state of the system. Therefore, in this section we build on the offline contracts and capacity budgets, and design an online service scheduling mechanism that dynamically refines SD–SP associations and resource allocation so as to adapt to the current system state.

In particular, we model the online service scheduling through interactions among two players: (i) SPs (e.g., ESs and APs), collected as $\mathcal{S}^{\text{on}} = \{s_1^{\text{on}}, \dots, s_i^{\text{on}}, \dots, s_{|\mathcal{S}^{\text{on}}|}^{\text{on}}\}$; and (ii) SDs (e.g., HUs and MUs), collected as $\mathcal{U}^{\text{on}} = \{u_1^{\text{on}}, \dots, u_j^{\text{on}}, \dots, u_{|\mathcal{U}^{\text{on}}|}^{\text{on}}\}$. In this stage, each SD strategically decides whether to execute its tasks locally or offload them to one of the available SPs, while SPs allocate their computing capacities to their associated tasks. Such mutually coupled decisions are then considered as a potential game. Specifically, to represent the offloading decision of u_j^{on} , we define the following binary indicator vector:

$$\mathbf{X}_j^{\text{on}} = (x_{j,0}^{\text{on}}, x_{j,1}^{\text{on}}, \dots, x_{j,i}^{\text{on}}, \dots, x_{j,|\mathcal{S}^{\text{on}}|}^{\text{on}}) \in \{0, 1\}^{1+|\mathcal{S}^{\text{on}}|}, \quad (9)$$

where $x_{j,0}^{\text{on}} = 1$ indicates local task execution at u_j^{on} and $x_{j,i}^{\text{on}} = 1$ indicates offloading to SP s_i^{on} (note that $\sum_{i=0}^{|\mathcal{S}^{\text{on}}|} x_{j,i}^{\text{on}} = 1, \forall j$). Given the profile \mathbf{X}_j^{on} , the resulting delays and costs are jointly determined by how many SDs concurrently choose the same SP and how its computing resources are shared. We next formalize this joint effect through a delay and congestion model, which will serve as the basis for defining the utilities of SDs and SPs.

5.1 Utility of SDs and SPs

5.1.1 Delay and Congestion Model

We consider the SP set \mathcal{S}^{on} and the SD set $\mathcal{U}^{\text{on}} = \mathcal{U}^{\text{H}} \cup \mathcal{U}^{\text{M}}$, where \mathcal{U}^{H} and \mathcal{U}^{M} denote the sets of HUs and MUs, respectively, where each SP s_i^{on} has a finite computing capacity $f_i^{\text{on}} > 0$ (CPU cycles/s). When a subset of SDs $\mathcal{U}_i = \{u_v^{\text{on}} \in \mathcal{U}^{\text{on}} : x_{v,i}^{\text{on}} = 1\}$ simultaneously offload their workload to s_i^{on} , the SP must multiplex its limited computing resource among heterogeneous requests with different priorities and contract terms. To capture both congestion effects and differentiated service levels in a tractable way, we adopt a weighted processor sharing (WPS) rule [13]: each SD u_j^{on} associated with s_i^{on} is assigned a positive weight $\gamma_{j,i} > 0$ that

reflects its service priority, contract tier, or fairness quota. The effective computing rate that u_j^{On} receives from s_i^{On} is then given by $\hat{f}_{j,i} = f_i^{\text{On}} \frac{\gamma_{j,i}}{\sum_{u_j^{\text{On}} \in \mathcal{U}_i^{\text{On}}} \gamma_{v,i}}$, and the corresponding edge-side computing delay can be obtained as:

$$t_{j,i}^{\text{comp}} = \frac{r_j}{\hat{f}_{j,i}} = \frac{r_j}{\gamma_{j,i}} \times \frac{\sum_{u_j^{\text{On}} \in \mathcal{U}_i^{\text{On}}} \gamma_{v,i}}{f_i^{\text{On}}}, \quad (10)$$

where r_j denotes the computing workload (e.g., CPU cycles needed) of u_j^{On} . This WPS model compactly captures how the delay of each SD grows with the aggregate load at the SP. We further summarize the impact of associated SDs on s_i^{On} through an *effective congestion load* defined as $y_i = \sum_{u_j^{\text{On}} \in \mathcal{U}_i^{\text{On}}} \gamma_{v,i}$. With this notation, (10) can be written in a factorized form as:

$$t_{j,i}^{\text{comp}} = \theta_{j,i} \tau_i(y_i), \quad \theta_{j,i} = \frac{r_j}{\gamma_{j,i}}, \quad \tau_i(y) = \frac{y}{f_i^{\text{On}}}, \quad (11)$$

where $\theta_{j,i}$ is a user-specific load factor, whereas $\tau_i(y)$ captures the server-side congestion effect as a function of the aggregate load. This separable structure will be instrumental for constructing an ordinal potential in the subsequent analysis.

While (11) characterizes the congestion-induced computing delay, an offloading SD also experiences wireless transmission latency in the uplink: when u_j^{On} offloads to s_i^{On} , the uplink delay is $t_{j,i}^{\text{tx}} = \frac{d_j}{W \log_2(1 + e_j^{\text{tx}} \Gamma_{j,i})}$, where d_j is the input data size, W is the bandwidth, e_j^{tx} is the transmit power, and $\Gamma_{j,i}$ is the Signal-to-Noise-Ratio (SNR) between u_j^{On} and s_i^{On} . Consequently, the total edge-side latency experienced by u_j^{On} when uploading its workload to s_i^{On} is given by:

$$T_{j,i}^{\text{edge}} = t_{j,i}^{\text{comp}} + t_{j,i}^{\text{tx}}. \quad (12)$$

5.1.2 Utility of HUs

Building on the above latency and energy models, we now characterize the utility of an HU when deciding whether to execute a task locally or offload it to an SP. Consider an HU $u_j^{\text{On}} \in \mathcal{U}^{\text{H}}$ with local CPU frequency f_j^{loc} and local computational power e_j^{loc} . The local execution time and energy consumption of its task are given by $t_j^{\text{loc}} = r_j / f_j^{\text{loc}}$ and $E_j^{\text{loc}} = r_j e_j^{\text{loc}} / f_j^{\text{loc}}$, respectively. When the HU u_j^{On} offloads its task to s_i^{On} , it experiences latency $t_{j,i}^{\text{comp}} + t_{j,i}^{\text{tx}}$ and uplink energy $E_{j,i}^{\text{tx}}$. Compared with local task execution, this leads to the latency saving of $t_{j,i}^{\text{save}} = t_j^{\text{loc}} - (t_{j,i}^{\text{comp}} + t_{j,i}^{\text{tx}})$ and energy saving of $c_{j,i}^{\text{save}} = E_j^{\text{loc}} - E_{j,i}^{\text{tx}}$ ($E_{j,i}^{\text{tx}}$ denotes the uplink transmission energy).

To map these latency and energy savings into a scalar benefit, we introduce non-negative valuation coefficients \mathbb{V}_t^{H} and \mathbb{V}_e^{H} to capture HU sensitivities to latency and energy, respectively. The HU's perceived valuation of being served by s_i^{On} is then modeled via $v_{j,i}^{\text{H}} = \mathbb{V}_t^{\text{H}} t_{j,i}^{\text{save}} + \mathbb{V}_e^{\text{H}} c_{j,i}^{\text{save}}$. Given this valuation, the HU's net utility must also account for the service payment: if s_i^{On} charges a price $p_{j,i}$ for serving u_j^{On} , its net utility is

$$U_{j,i}^{\text{H}} = v_{j,i}^{\text{H}} - p_{j,i}, \quad U_{j,0}^{\text{H}} = 0, \quad (13)$$

where the value of $U_{j,0}^{\text{H}}$ corresponds to local task execution.

5.1.3 Utility of MUs

While HUs mainly care about the joint latency–energy tradeoff, MUs (e.g., robots or sensing devices) are typically driven by task deadlines and reliability requirements. We therefore adopt a slightly different utility structure for MUs. Specifically, an MU $u_j^{\text{On}} \in \mathcal{U}^{\text{M}}$ is associated with a latency

deadline τ_j^{ddl} , while its total edge-side latency at s_i^{On} is $T_{j,i}^{\text{edge}}$ in (12). To capture the fact that the MU primarily values meeting this deadline, we adopt a *soft-deadline* valuation

$$G_{j,i}^{\text{M}} = v_j [\tau_j^{\text{ddl}} - T_{j,i}^{\text{edge}}]_+ \times (\tau_j^{\text{ddl}})^{-1}, \quad (14)$$

where $[x]_+ = \max\{x, 0\}$ and $v_j > 0$ denotes the MU's task reward. Intuitively, the MU obtains the full reward v_j if the deadline is met, whereas excessive latency leads to a loss of reward (once the deadline is violated, the reward becomes zero). In particular, "soft-deadline" means that this reward decreases smoothly as latency approaches the deadline, instead of dropping abruptly from full reward to zero at a hard threshold.

In addition to timeliness, an MU also benefits from saving local computing energy by task offloading. Similar to HUs, the MU's energy saving when utilizing edge services is $c_{j,i}^{\text{M,save}} = E_j^{\text{loc}} - E_{j,i}^{\text{tx}}$, where E_j^{loc} is the local execution energy and $E_{j,i}^{\text{tx}}$ is the uplink transmission energy. Let \mathbb{V}_e^{M} denote the MU's valuation coefficient on energy saving. Combining deadline satisfaction, energy saving, and the service payment $p_{j,i}$, the MU's utility when transferring its tasks to s_i^{On} can be given by:

$$U_{j,i}^{\text{M}} = G_{j,i}^{\text{M}} + \mathbb{V}_e^{\text{M}} c_{j,i}^{\text{M,save}} - p_{j,i}, \quad U_{j,0}^{\text{M}} = 0, \quad (15)$$

where $U_{j,0}^{\text{M}}$ corresponds to local task execution.

Note that both HU and MU utilities in (13) and (15) inherently share the same congestion component $t_{j,i}^{\text{comp}} = \theta_{j,i} \tau_i(y_i)$ in (11). This shared structure will be crucial for aligning individual incentives with system-wide performance via an ordinal potential function in our subsequent analysis (Sec. 5.2).

5.1.4 Cost of SPs

Having specified how HUs and MUs (i.e., SDs) evaluate edge services, we now focus on the SPs' perspective. As more SDs offload their tasks to an SP, the SP consumes more energy and experiences higher operating costs, which must be reflected in its payoff and, ultimately, in the system-level SW. Subsequently, for each SP s_i^{On} , given its aggregated computing load $\mathbb{x}_i = \sum_{u_j^{\text{On}} \in \mathcal{U}_i^{\text{On}}} r_{v,i}$, we model its computation/operation cost as follows:

$$K_i(\mathbb{x}_i) = \omega_1 e_i^{\text{comp}} \mathbb{x}_i / f_i^{\text{On}} + \omega_2 c^{\text{hard}}, \quad (16)$$

where e_i^{comp} is the average computing power consumption of s_i^{On} , and c^{hard} captures hardware- and maintenance-related costs ($\omega_1, \omega_2 \geq 0$ are weighting coefficients). In (16), the term proportional to $\mathbb{x}_i / f_i^{\text{On}}$ reflects that processing a larger workload leads to higher energy and operational expenditure. It is worth noting that although an SP may collect service payments $\sum_{u_j^{\text{On}} \in \mathcal{U}_i^{\text{On}}} p_{v,i}$, these payments are monetary transfers among SP and SDs and therefore cancel out when aggregating the system-level SW. Consequently, they do not appear in the potential function constructed later in Sec. 5.2 and only affect how the SW is divided among SPs and SDs.

In a nutshell, in our considered human–machine ecosystem, SPs resources are limited and SDs (i.e., HUs/MUs) act selfishly, where each SD tries to choose the execution mode of its tasks (local vs. offloading) and SP that maximizes its own utility. Directly coordinating all the coupled decisions across SPs and SDs via a centralized SW maximization formulation is computationally prohibitive and poorly scalable. This motivates our following game-theoretic treatment in which we capture the system performance by a carefully crafted

potential function that is aligned with individual incentives and allows for decentralized handling of resource allocations across SPs and SDs.

5.2 Ordinal Potential Function

In order to analyze our online resource scheduling game and to enable simple distributed best-response dynamics with provable convergence, we first construct an *ordinal potential* $\Phi(\pi)$ that aggregates SD-side benefits and SP-side costs. This construction leverages the unified congestion structure in (11) together with the above-described deadline-aware MUs' utilities.

For an MU u_j^{On} served by s_i^{On} , the time-related part of its payoff was modeled by the soft-deadline valuation in (14) as $G_{j,i}^{\text{M}} = v_j [\tau_j^{\text{ddl}} - T_{j,i}^{\text{edge}}]_+ \times (\tau_j^{\text{ddl}})^{-1}$. This valuation, together with energy saving and the payment term, determines the MU's overall utility in the online game defined in (15). We note that since the computing delay $t_{j,i}^{\text{comp}}$ in (11), which is inherently encoded in (15), is an increasing function of the congestion load y_i , heavier congestion directly reduces $G_{j,i}^{\text{M}}$ and the utility in (11). This monotone relationship between congestion and MU valuation allows us to align individual best responses with the system-wide potential in the subsequent analysis.

For HUs, the utility in (13) can be decomposed into a congestion-independent valuation part and a congestion-dependent penalty, as follows:

$$U_{j,i}^{\text{H}} = \underbrace{\mathbb{V}_t^{\text{H}}(t_j^{\text{loc}} - t_{j,i}^{\text{tx}})}_{S_j(i) \text{ (valuation independent of } y_i)} + \underbrace{\mathbb{V}_e^{\text{H}}(E_j^{\text{loc}} - E_{j,i}^{\text{tx}})}_{\text{congestion penalty}} - p_{j,i}, \quad (17)$$

where $S_j(i)$ collects all valuation terms that do not depend on the congestion load y_i , while the second term captures how queueing-induced delay degrades the HU's utility. Note that the payment $p_{j,i}$ is also independent of y_i , but is written separately because it represents a monetary transfer, which will cancel out at the system level in our subsequent potential analysis.

MU utilities also admit the same structural form: by linearizing $G_{j,i}^{\text{M}}$ around typical delay levels (see Appx. D.4), the MU utility can be rewritten as:

$$U_{j,i}^{\text{M}} = \bar{S}_j(i) - \kappa_j \theta_{j,i} \tau_i(y_i) - p_{j,i}, \quad (18)$$

where $\bar{S}_j(i)$ gathers the non-congestion valuation terms (soft-deadline valuation base reward and energy saving), and $\kappa_j > 0$ reflects the MU's effective sensitivity to congestion. Similar to (17), $p_{j,i}$ is separated from $\bar{S}_j(i)$ in (18) even though it does not depend on y_i , so that monetary transfers can be excluded from the system-level potential.

Considering both HUs and MUs, the utility of SD $u_j^{\text{On}} \in \mathcal{U}^{\text{On}}$ when it is served by $s_i^{\text{On}} \in \{0\} \cup \mathcal{S}^{\text{On}}$ can be unified as follows:

$$U_{j,i} = S_j(i) - \kappa_j \theta_{j,i} \tau_i(y_i) - p_{j,i}, \quad (19)$$

where $i = 0$ corresponds to local task execution at SD u_j^{On} and $S_j(0) = 0$. In (19), $S_j(i)$ encodes the non-congestion valuation terms (latency/energy saving or soft-deadline valuation), $\kappa_j \theta_{j,i}$ captures how sensitive u_j^{On} is to the congestion at s_i^{On} , and $\tau_i(\cdot)$ is the server-side congestion function that only applies when $i \in \mathcal{S}^{\text{On}}$ (local execution does not impact edge-side congestion). The term $p_{j,i}$ represents the payment charged to u_j^{On} and, while independent of congestion, is written explicitly as it will later be treated as a monetary transfer in the system-level analysis. The

unified representation in (19) captures SD (i.e., HU/MU) heterogeneity through $(S_j, \kappa_j, \theta_{j,i})$, whereas all SDs are coupled through the same congestion mechanism $\tau_i(y_i)$ at each SP.

To describe how individual decisions interact at the system-level, we collect all SD assignments into the *joint assignment profile*⁵ $\pi = (\pi_j)_{j \in \mathcal{U}^{\text{On}}}$, where $\pi_j \in \{0\} \cup \mathcal{S}^{\text{On}}$ denotes the choice of u_j^{On} : $\pi_j = 0$ means that the task is processed locally at u_j^{On} , while $\pi_j = i$ indicates task offloading to SP s_i^{On} . Given a profile π , we can then compute, for each SP s_i^{On} , the effective congestion load and the physical computing load as follows:

$$y_i(\pi) = \sum_{j: \pi_j = i} \gamma_{j,i}, \quad \mathbb{x}_i(\pi) = \sum_{j: \pi_j = i} r_j, \quad (20)$$

where $y_i(\pi)$ feeds into the congestion-induced delay via $t_{j,i}^{\text{comp}} = \theta_{j,i} \tau_i(y_i(\pi))$ in (11), and $\mathbb{x}_i(\pi)$ determines the SP-side computation/operation cost through $K_i(\mathbb{x}_i(\pi))$ in (16). Thus, any unilateral change of π_j only modifies the loads of the involved SPs in (20), and these updated loads propagate to SD delays and SP costs through (11) and (16), respectively.

In order to analyze the resulting game and to show that simple myopic best-response updates can converge, we now construct an *ordinal potential function* that aggregates both SD-side benefits and SP-side costs as follows:

$$\Phi(\pi) = \underbrace{\sum_{j: \pi_j \neq 0} S_j(\pi_j)}_{\text{user-side non-congestion benefits}} - \underbrace{\sum_{i \in \mathcal{S}^{\text{On}}} \int_0^{y_i(\pi)} \tau_i(z) dz}_{\text{aggregated congestion cost}} - \underbrace{\sum_{i \in \mathcal{S}^{\text{On}}} K_i(\mathbb{x}_i(\pi))}_{\text{SP computation/operation cost}}, \quad (21)$$

where the first term sums up the non-congestion valuation of all SDs that choose to offload, the second term integrates the congestion function $\tau_i(\cdot)$ from zero to the realized load $y_i(\pi)$ across SPs, and the last term captures the cost of running edge resources. By jointly accounting for SD-side benefits, congestion penalties, and SP-side costs, $\Phi(\pi)$ serves as a system-level measure whose variations mirror individual utility changes; this coupling is key to proving that our online resource scheduling game is an ordinal potential game and that distributed better/best-response dynamics converge to a pure-strategy NE. In particular, consider a unilateral deviation where one SD u_j^{On} switches from SP s_i^{On} to another SP $s_{i'}^{\text{On}}$ (or to local task execution). The resulting change in $\Phi(\pi)$ can be decomposed as follows:

- **User-side non-congestion term:** The first term in (21) only depends on the non-congestion valuation $S_j(\cdot)$ of the deviating SD, while all other SDs keep the same assignment. Hence, its increment is exactly the change in that SD's non-congestion benefit, i.e., $S_j(\pi_j^{\text{new}}) - S_j(\pi_j^{\text{old}})$.
- **Congestion term:** The second term aggregates the integrated congestion at each SP through $\int_0^{y_i(\pi)} \tau_i(z) dz$, where $\tau_i(y)$ is an increasing function of the congestion load y (recall $\tau_i(y) = y/f_i^{\text{On}}$). When u_j^{On} moves from s_i^{On} to $s_{i'}^{\text{On}}$ (or from/to local execution), the loads y_i and $y_{i'}$ change by fixed amounts. Because $\tau_i(\cdot)$ and $\tau_{i'}(\cdot)$ are increasing functions and $\kappa_j \theta_{j,i} > 0$, the sign of the change in the integrated congestion term matches the sign of the change in that SD's congestion penalty $\kappa_j \theta_{j,i} \tau_i(y_i)$; this follows the

5. Given π , the binary indicators $x_{j,i}^{\text{On}}$ are induced by $x_{j,i}^{\text{On}} = \mathbb{1}_{\{\pi_j = i\}}$, $i \in \{0\} \cup \mathcal{S}^{\text{On}}$ ($\mathbb{1}_{\{\cdot\}}$ denotes the binary indicator function), so that the vector \mathbf{X}_j^{On} and the scalar action π_j are equivalent representations of u_j^{On} 's decision.

standard integral–pointwise comparison used in congestion games [27].

- **SP-side cost term:** The third term in (21) captures the SP-side computation/operation cost $K_i(\mathbb{x}_i(\boldsymbol{\pi}))$, where $\mathbb{x}_i(\boldsymbol{\pi})$ is the aggregate computing load at s_i^{On} . A deviation by u_j^{On} only changes the loads at s_i^{On} and $s_{i'}^{\text{On}}$, and, due to the convex and increasing behavior of $K_i(\cdot)$ with respect to \mathbb{x}_i , the sign of the change in this term is aligned with the way that the SD's action changes the corresponding SP-side cost.

Putting the above components together, it can be immediately construed that whenever u_j^{On} changes its action in a way that strictly increases its own utility (excluding the payment term $p_{j,i}$), the resulting change in $\Phi(\boldsymbol{\pi})$ has the same sign as its utility improvement. In other words, $\Phi(\boldsymbol{\pi})$ is an *ordinal potential* for our online resource scheduling game under the soft-deadline valuations: any unilateral utility-improving deviation by an SD strictly increases $\Phi(\boldsymbol{\pi})$. This property is crucial as it implies that simple distributed better-/best-response dynamics monotonically climb the potential and therefore converge in finitely many steps to a pure-strategy NE. In particular, we mathematically prove that $\Phi(\boldsymbol{\pi})$ in (21) is an ordinal potential, so that any unilateral utility-improving move strictly increases $\Phi(\boldsymbol{\pi})$ and any better-/best-response dynamics converge to a pure-strategy NE (see Appx. C for details); the complete technical development, including the matrix reformulation, the integral–pointwise “sandwich” inequality, and the finite-improvement property, is deferred to Appx. D.

5.3 Problem Formulation

In this online stage, our goal is to coordinate the task offloading decisions of heterogeneous SDs (i.e., MUs/HUs) and the admission decisions of SPs, while respecting coverage and subcarrier-capacity constraints. To this end, following our above discussions, we utilize the fact any maximizer of $\Phi(\boldsymbol{\pi})$ corresponds to a pure-strategy NE that balances SD-side benefits and SP-side costs under congestion, and subsequently formulate the online scheduling problem as $\mathcal{F}^{(\text{II})}$:

$$\mathcal{F}^{(\text{II})} : \underset{\boldsymbol{\pi}}{\operatorname{argmax}} \Phi(\boldsymbol{\pi}) \quad (22)$$

$$\text{s.t. } \pi_j \in \{0\} \cup \mathcal{S}^{\text{On}}, \quad \forall u_j^{\text{On}} \in \mathcal{U}^{\text{On}}, \quad (22a)$$

$$x_{j,i}^{\text{On}} = 0, \quad \text{if } s_i^{\text{On}} \notin \mathcal{C}_j, \quad \forall u_j^{\text{On}} \in \mathcal{U}^{\text{On}}, \quad (22b)$$

$$\sum_{u_j^{\text{On}} \in \mathcal{U}^{\text{On}}} x_{j,i}^{\text{On}} \leq G_i, \quad \forall s_i^{\text{On}} \in \mathcal{S}^{\text{On}}, \quad (22c)$$

where $\boldsymbol{\pi} = (\pi_j)_{j \in \mathcal{U}^{\text{On}}}$ denotes the joint assignment profile, with $\pi_j = 0$ representing local task execution at u_j^{On} and $\pi_j = i$ indicating task offloading to SP s_i^{On} . The binary variables $x_{j,i}^{\text{On}}$ are induced by $\boldsymbol{\pi}$ as defined in Sec. 5.2 (i.e., $x_{j,i}^{\text{On}} = 1$ if $\pi_j = i$).

Constraint (22a) enforces each SD to choose only one execution option for its current task: either local processing ($\pi_j = 0$) or offloading to a single SP ($\pi_j \in \mathcal{S}^{\text{On}}$). Constraint (22b) captures the service-coverage feasibility: \mathcal{C}_j denotes the set of SPs that can physically serve u_j^{On} (e.g., within communication range), and thus the association variable for an SD outside the coverage of s_i^{On} is forced to zero. Constraint (22c) limits the admission load at each SP, where G_i is the maximum number of SDs that SP s_i^{On} can concurrently serve.

Problem $\mathcal{F}^{(\text{II})}$ is an integer programming (IP) problem over a discrete action space and is, in general, NP-hard. Since this online scheduling has to be repeatedly solved at each trading round under stringent latency and computational constraints at the edge, running a centralized IP solver or heavyweight meta-heuristics to seek a global optimum is impractical. Instead, by recasting $\mathcal{F}^{(\text{II})}$ as an ordinal potential game and constructing the potential function $\Phi(\boldsymbol{\pi})$, we obtain a formulation that admits a fully-distributed implementation. In particular, it can be shown that a simple better-/best-response strategy (described in Sec. 5.4), where each SD myopically maximizes its own utility subject to feasibility, monotonically increase $\Phi(\boldsymbol{\pi})$ and converge in finitely many steps to a pure-strategy NE (see Appx. C for details), which serves as a locally optimal and practically attainable solution to (22).

5.4 Potential-Guided Best-Response Dynamics (PG-BRD)

For brevity, we provide the complete pseudo-code of PG-BRD in Alg. 3 and summarize its four main steps below:

Step 1. Random-feasible initialization (lines 1-2, Alg. 3): We first construct a feasible initial association profile $\boldsymbol{\pi}^{(0)} \in \{0, 1, \dots, |\mathcal{S}^{\text{On}}|\}^{|\mathcal{U}^{\text{On}}|}$, where $\pi_j = 0$ corresponds to local task execution at u_j^{On} and $\pi_j = i > 0$ means that u_j^{On} offloads its task to SP s_i^{On} . For each SD u_j^{On} , we randomly select an action from the set $\{0\} \cup \mathcal{C}_j$ and only accept it if the resulting profile satisfies the coverage constraint (22b) and the subcarrier-capacity constraint (22c). This procedure ensures that the algorithm starts from a valid resource scheduling configuration with no constraint violations.

Step 2. Feasible-action enumeration under coverage and subcarrier-capacity constraints (lines 7-9, Alg. 3): Given a current profile $\boldsymbol{\pi}$, we compute for each SP s_i^{On} the effective congestion load $y_i(\boldsymbol{\pi})$ and the physical computing load $\mathbb{x}_i(\boldsymbol{\pi})$ as in (20), as well as the number of currently served SDs $n_i(\boldsymbol{\pi}) = |\{j \mid \pi_j = i\}|$. When it is SD u_j^{On} 's turn to update

Algorithm 3: Proposed PG-BRD

- 1 **Input:** SD set \mathcal{U}^{On} , SP set \mathcal{S}^{On} , coverage sets $\{\mathcal{C}_j\}$, subcarrier-capacity $\{G_i\}$, max iterations T_{\max} , threshold ε .
 - 2 **Initialization:** Construct a random feasible profile $\boldsymbol{\pi} = (\pi_j)_{j \in \mathcal{U}^{\text{On}}}$ that satisfies constraints (22a)–(22c); set $t \leftarrow 0$ and converged \leftarrow **false**.
 - 3 **while** not converged **and** $t < T_{\max}$ **do**
 - 4 converged \leftarrow **true**;
 - 5 Generate a random permutation \mathcal{P} of indices in \mathcal{U}^{On} ;
 - 6 **for each** SD u_j^{On} in \mathcal{P} **do**
 - 7 let $a_j^{\text{cur}} \leftarrow \pi_j$;
 - 8 for all i , compute the loads excluding u_j^{On} : y_i^{-j} , \mathbb{x}_i^{-j} , and n_i^{-j} ;
 - 9 build the feasible action set $\mathcal{A}_j^{\text{feas}}$ according to (23);
 - 10 compute current utility $U_j(a_j^{\text{cur}} \mid \boldsymbol{\pi}_{-j})$ via (19);
 - 11 **for each** $a \in \mathcal{A}_j^{\text{feas}}$ **do**
 - 12 temporarily set $\pi_j \leftarrow a$ and evaluate $U_j(a \mid \boldsymbol{\pi}_{-j})$;
 - 13 let $a_j^{\text{best}} \in \operatorname{argmax}_{a \in \mathcal{A}_j^{\text{feas}}} U_j(a \mid \boldsymbol{\pi}_{-j})$;
 - 14 **if** $U_j(a_j^{\text{best}} \mid \boldsymbol{\pi}_{-j}) - U_j(a_j^{\text{cur}} \mid \boldsymbol{\pi}_{-j}) > \varepsilon$ **then**
 - 15 $\pi_j \leftarrow a_j^{\text{best}}$;
 - 16 converged \leftarrow **false**;
 - 17 **else**
 - 18 $\pi_j \leftarrow a_j^{\text{cur}}$;
 - 19 $t \leftarrow t + 1$;
 - 20 **Output:** NE profile $\boldsymbol{\pi}^* = \boldsymbol{\pi}$ and the associated allocation.
-

its decision, we temporarily remove its own contribution and obtain the loads generated by all other SDs, denoted by y_i^{-j} , x_i^{-j} , and n_i^{-j} . These quantities represent the congestion level and computing load at each SP if u_j^{On} were not associated with any SP. Given these congestion and load levels generated by all other SDs, we construct the feasible action set for u_j^{On} as follows:

$$A_j^{\text{feas}} = \left\{ a \in \{0\} \cup S^{\text{On}} \mid a = 0 \text{ or } (a = i > 0, s_i^{\text{On}} \in C_j, n_i^{-j} + 1 \leq G_i) \right\}, \quad (23)$$

where $a = 0$ corresponds to local task execution, and an offloading action $a = i > 0$ is feasible only if SP s_i^{On} covers u_j^{On} and still has enough residual subcarrier-capacity to admit one more SD without violating its capacity G_i . This step explicitly removes any candidate action that would break either the coverage or the subcarrier-capacity constraints.

Step 3. Asynchronous best response under the ordinal potential (lines 10-18, Alg. 3): In each iteration, SDs are visited one-by-one in a random order, and at most one SD is allowed to change its decision at a time. For a given SD u_j^{On} and current profile π , we first evaluate its current utility $U_j(\pi_j \mid \pi_{-j})$ using the unified expression in (19). Then, for each feasible action $a \in A_j^{\text{feas}}$, we temporarily set $\pi_j = a$, recompute the congestion and delay quantities for this SD, and obtain the resulting utility $U_j(a \mid \pi_{-j})$. The SD then chooses a best response $a_j^{\text{best}} \in \arg \max_{a \in A_j^{\text{feas}}} U_j(a \mid \pi_{-j})$. To avoid frequent switches caused by marginal gains, we introduce an acceptance threshold $\varepsilon > 0$ and let u_j^{On} update its decision only if $U_j(a_j^{\text{best}} \mid \pi_{-j}) - U_j(\pi_j \mid \pi_{-j}) > \varepsilon$. Otherwise, it keeps its current action π_j unchanged. Because the game admits the ordinal potential $\Phi(\pi)$, every accepted update in this step strictly increases $\Phi(\pi)$.

Step 4. Convergence and resulting equilibrium (lines 3-20, Alg. 3): The above two steps (feasible-action enumeration and asynchronous best responses) are repeatedly applied by going over all SDs. When a complete pass over \mathcal{U}^{On} produces no accepted update, no SD can improve its utility by more than ε through a unilateral change of its action, and thus a pure-strategy NE π^* is reached.

6 EVALUATIONS

We next conduct numerical experiments to evaluate FUSION. We consider a service provisioning region of size $1000 \text{ m} \times 1000 \text{ m}$, where ESs are randomly placed (HUs and MUs are in turn randomly placed within the coverage areas of ESs) and APs can be dispatched to assist overloaded ESs. The availability windows of ESs are randomly generated over a normalized time horizon to capture the temporal variability of computation demand. Other key parameters are as follows [22], [25], [30]: $f_i^{\text{E}} \in [1, 3] \times 10^{12}$ CPU cycles/s (this is the aggregated clock speed of CPUs co-located at the ES), $f_k^{\text{A}} \in [1, 3] \times 10^{10}$ CPU cycles/s, $f_m^{\text{H,loc}} = f_n^{\text{M,loc}} \in [1, 2] \times 10^9$ CPU cycles/s, $d_m^{\text{H}} \in [10, 55]$ Mbit, $d_n^{\text{M}} \in [100, 550]$ Mbit, $G_i \in [6, 8]$, $G_k^{\text{A}} \in [1, 2]$, $C_k^{\text{A}} \in [8, 10]$, $W = 50$ MHz, $e_m^{\text{H,tx}} = e_n^{\text{M,tx}} = e_k^{\text{A,tx}} \in [0.2, 0.4]$ W, $r_m^{\text{H}} = 600$ cycles/bit $\times d_m^{\text{H}}$, and $r_n^{\text{M}} = 600$ cycles/bit $\times d_n^{\text{M}}$. Channel gains and data rates are generated using the distance-dependent path-loss models following [31]. Under these models, most links fall into an SNR range of 10–25 dB, and UAV links achieve slightly higher average SNR due to their higher Line-of-Sight (LoS) probability. All figures are obtained via Monte-Carlo method over 100 independent trials.

6.1 Benchmark Methods and Evaluation Metrics

We evaluate FUSION from two complementary angles: (i) prediction performance on service demand forecasting module (Sec. 6.2); and (ii) system-level performance (Sec. 6.3).

6.1.1 Benchmarks and Metrics for Demand Forecasting

We compare Pro-LNN against two widely used prediction models.

- **LSTM-driven demand prediction [28]:** A standard long short-term memory (LSTM) network is applied to the input sequences $\{z_i\}$ and trained to predict future ES demands. This baseline represents a strong discrete-time RNN model.

- **Transformer-driven demand prediction [29]:** A temporal Transformer-based predictor with self-attention is used over the historical context window. This serves as a powerful baseline, but typically requires more computing resources.

Performance evaluations consider the following metrics:

- **Accuracy:** We report the root mean square error (RMSE), mean absolute error (MAE), and symmetric mean absolute percentage error (sMAPE) of the H -step forecasts $\{\hat{N}_i^{\text{Dem},(\nu+1:\nu+H)}\}$ against the ground truth $\{N_i^{\text{Dem},(\nu+1:\nu+H)}\}$, averaged over all ESs and all test instances.

- **Model footprint:** We measure the total number of trainable parameters and the corresponding 32-bit floating-point format (FP32, measured in megabytes) for each predictor, which together characterize its computing (memory/storage) overhead.

- **Robustness:** To assess robustness under realistic noisy conditions, we compare the mean squared error (MSE) on clean test inputs with that on corrupted inputs containing randomly missing observations, additive perturbations, and occasional demand bursts, and report the performance drop ΔMSE .

6.1.2 System-Level Benchmarks and Metrics

We then compare FUSION with several benchmark methods enumerated below:

- **Pure online scheduling (PurOnline) [13]:** This baseline removes the offline stage of FUSION completely, e.g., ESs and APs do not sign any offline contracts, and UAV locations are not pre-planned. All HUs and MUs directly enter the online market, where their tasks are scheduled only via the PG-BRD-based scheduling over the current ES/AP network environment.

- **Two-stage resource provisioning without PG-based online scheduling (FUSION_NoPG):** This variant keeps the same offline stage as FUSION, i.e., Off-AIC² with eACO-VRP is still used to form offline AP-ES contracts and pre-planned routes. However, the online stage abandons PG-BRD: HU/MU tasks are randomly assigned to feasible ESs/APs within coverage subject to resource capacity and deadline constraints.

- **Two-stage resource provisioning with random offline contracts (FUSION_Random):** This baseline uses the same online stage as FUSION and still relies on PG-BRD for congestion-aware online resource scheduling. However, its offline stage no longer uses Off-AIC² or eACO-VRP; instead, each AP is randomly associated with a subset of ESs and moves along a random feasible route until its capacity is exhausted.

- **Two-stage resource provisioning without ES spatio-temporal features (FUSION_NoST):** This baseline preserves the two-stage structure of FUSION, but its offline auction ignores ES-specific time windows and travel-time constraints. Specifically, AP-ES pairs are determined only by simple price/volume trading without using eACO-VRP, while online stage still runs PG-BRD for task scheduling.

To assess performance, we use the following metrics:

- **Social welfare (SW):** SW captures the sum of utilities of all ESs, APs, and users across both stages: in the offline stage, SW accounts for ES profits, AP utilities, and auctioneer surplus given by (1)-(3); in the online stage, it captures the potential value $\Phi(\pi)$, combining SD-side benefits and SP-side costs.
- **Delay incurred by interactions between SPs and SDs (DoI):** DoI captures the total decision-making latency (in milliseconds) induced by control-message exchanges between ESs/APs (SPs) and HUs/MUs (SDs) across both offline and online stages. To compute DoI, following [30], [32], [33], we assume that the per-interaction delay lies in the range of [1, 15] ms.
- **Energy consumption incurred by interactions between SPs and SDs (ECoI):** ECoI measures the signaling-related energy consumption during the decision-making process. To compute ECoI, we assume that the transmit power of ESs lies in [6, 20] W, consistent with [30], [32]. Specifically, ECoI is obtained by aggregating the energy consumed by all control-message transmissions and the corresponding interaction delays.
- **Truthfulness and individual rationality of Off-AIC²:** To empirically verify the economic properties of Off-AIC², we conduct a set of experiments in which ESs and APs are allowed to deviate from their truthful bids/asks. We measure the proportion of ESs and APs whose utilities increase under such deviations. An auction that is truthful and individually rational should ensure that (i) every winning ES attains a non-negative utility and cannot benefit from misreporting its bid, and (ii) every winning AP receives a payment no lower than its declared ask and gains no advantage by inflating or deflating it.

6.2 Performance Evaluation on Prediction

6.2.1 Robustness vs. Cost

We first conduct experiments to evaluate “robustness vs. cost” trade-off in Table 2. In the “clean” setting, we feed each model with intact historical sequences, while in the “corrupt” setting, we inject 30% random missing values, additive Gaussian noise with standard deviation $\sigma = 0.05$, and random burst shocks of length 1–3. On clean data, LSTM attains the lowest MSE (0.119), whereas Transformer and Pro-LNN yield slightly larger errors (0.467 and 0.459, respectively). This gap is expected, as LSTM uses approximately 52.8k parameters, compared to only 11.1k parameters of Pro-LNN, implying significantly higher computation costs. Once corrupted inputs are introduced, however, LSTM error surges to 0.983 (a relative increase of +726.3%), while the errors of Transformer and Pro-LNN only grow to 0.781 and 0.762 (relative increases of +67.3% and +66.1%), respectively. These results indicate that our proposed Pro-LNN offers a favorable trade-off between robustness and cost compared to an over-parameterized LSTM on noisy sequences, which matches the characteristics of ES demand trajectories in Off-AIC².

TABLE 2

Robustness–complexity comparison of different forecasters on synthetic non-stationary series. The “corrupt” case injects 30% random missing values, Gaussian noise with standard deviation $\sigma = 0.05$, and random burst shocks.

Model	#Params	MSE _{clean}	MSE _{corrupt}	Δ MSE	Rel. increase
LSTM	52800	0.119	0.983	0.864	+726.3%
Transformer	69500	0.467	0.781	0.314	+67.3%
Pro-LNN	11100	0.459	0.762	0.303	+66.1%

6.2.2 Real-World Dataset Test

We validate Pro-LNN on the UCI Electricity Load Diagrams 2011–2014 dataset [34] using two feeders (MT_005 and MT_145) in a univariate task, where a history of $T_{\text{his}} = 48$ past measurements predict the next $H = 10$ time steps. We use this dataset since the electricity load traces are commonly used as a proxy for computing service demand, since power consumption in ESs can be directly driven by processor utilization and exhibits similar diurnal and bursty temporal patterns. Quantitative results are summarized in Table 3 and Table 4. Observing Table 3, Pro-LNN achieves comparable prediction accuracy to LSTM and Transformer, while being much more compact. In particular, Pro-LNN attains an RMSE of 0.1234, close to that of the LSTM (0.1121) and the Transformer (0.1158), but only uses 11,114 parameters and has a 0.046 MB storage/memory footprint. This corresponds to roughly 4–6 \times fewer parameters and 4–9 \times smaller model size than other methods, signaling the deployability of our Pro-LNN over resource-constrained edge networks. To evaluate robustness, we inject corrupted inputs, following the same configuration as in the synthetic experiments detailed in Sec. 6.2.1. As reported in Table 4, Pro-LNN exhibits the smallest performance degradation among all models: its MSE increases from 0.0152 (clean) to 0.0467 (corrupt), yielding a Δ MSE of 0.0315, which is lower than that of both LSTM (0.0359) and Transformer (0.0458). These observations indicate that Pro-LNN is highly parameter-efficient and demonstrates strong robustness to missing data and measurement noise, which in turn supports the suitability of Pro-LNN for forecasting future ES resource demands in the offline stage of FUSION.

6.3 Performance Evaluation on FUSION

To emulate heterogeneous, time-varying online demands across different ESs, we adopt the real-world UCI Electricity Load Diagrams dataset [34], select several distinct load

TABLE 3

Prediction accuracy and model footprint on the UCI dataset (feeders MT_005 and MT_145, input length $T_{\text{his}} = 48$, prediction horizon $H = 10$).

Model	#Params	Size (MB)	RMSE	MAE	sMAPE
LSTM	52842	0.204	0.1121	0.0816	0.1831
Transformer	69482	0.400	0.1158	0.0824	0.1864
Pro-LNN	11114	0.046	0.1234	0.0906	0.1983

TABLE 4

Robustness to missing and noisy inputs on UCI Electricity (30% random missing values, added Gaussian noise with standard deviation of $\sigma = 0.05$, and random burst shocks).

Model	MSE (clean)	MSE (corrupt)	Δ MSE
LSTM	0.0126	0.0485	0.0359
Transformer	0.0134	0.0592	0.0458
Pro-LNN	0.0152	0.0467	0.0315

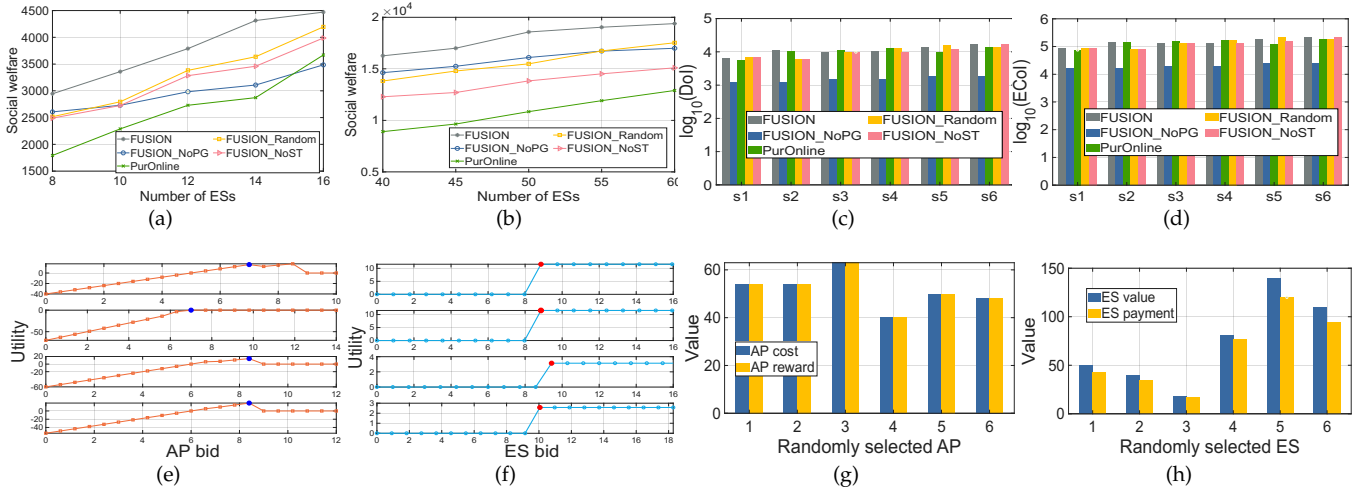


Fig. 2. Performance comparisons and economic property analyses, where (a)-(b) SW under different problem sizes (80 HUs, 80 MUs, and 5 APs in (a), and 400 HUs, 400 MUs, and 35 APs in (b)), (c)-(d) DoI and ECoI under different problem sizes (s1-s6 are set as $\{75/75/15/8\}$, $\{75/75/20/8\}$, $\{90/90/20/10\}$, $\{90/90/25/10\}$, $\{115/115/25/12\}$, and $\{115/115/30/12\}$), (e)-(f) truthfulness, and (g)-(h) individual rationality.

profiles, and map their normalized power-consumption traces to the per-time-slot resource demand of each ES. We then train Pro-LNN on these profiles to forecast the per-ES demand⁶, and then evaluate FUSION as follows (i.e., in Sec. 6.3.1–Sec. 6.3.3).

6.3.1 Social Welfare (SW)

Figs. 2(a)–2(b) report SW as the number of ESs increases from 8 to 16. The two subfigures correspond to two representative network configurations: 80 HUs, 80 MUs, and 5 APs in Fig. 2(a), and 400 HUs, 400 MUs, and 35 APs in Fig. 2(b) to capture different network scales.

In Fig. 2(a), SW increases for all methods as more ESs are introduced, since additional ESs provide more computing resources and service opportunities. However, the growth rates differ across schemes. FUSION consistently achieves the highest SW because its offline stage employs Off-AIC² to match AP resources with ESs of high revenue potential under spatio-temporal constraints, while its online stage adopts a PG-BRD scheduler to perform congestion-aware task allocation among HUs and MUs, leading to more efficient and fair resource utilization. PurOnline, which lacks an offline stage and relies solely on an online potential game over real-time ES resources, achieves the lowest SW due to the absence of proactive UAV repositioning. FUSION_NoPG shares the same offline design as FUSION but replaces PG-BRD with random online assignment, resulting in unresolved congestion and a notable SW degradation, highlighting the importance of the online PG. FUSION_Random adopts random AP-ES association in the offline stage while retaining PG-BRD online, yielding intermediate performance and indicating that intelligent online scheduling alone cannot compensate for the lack of revenue- and spatio-temporal-aware offline planning. FUSION_NoST ignores ES spatio-temporal characteristics in the offline stage and relies on a price-driven auction with PG-BRD online; it outperforms PurOnline and FUSION_Random but still exhibits a consistent gap to FUSION. Fig. 2(b) shows qualitatively similar trends under the larger-scale

6. We employ the UCI dataset as a trace to capture realistic temporal patterns of aggregate demand at each ES. Pro-LNN is trained on these time series and used to forecast the demand $N_i^{\text{Dem},(\nu)}$ of ES s_i over future trading rounds; the forecasted demand profiles drive the time-varying SD task-arrival intensities at each ES, while the total population sizes of SDs and SPs are kept fixed to control the overall network scale.

configuration: as the number of ESs increases, SW rises for all methods, with FUSION consistently outperforming the baselines. Overall, these results indicate that, in FUSION, a well-designed offline AP-ES contracting mechanism (particularly, Off-AIC² with explicit spatio-temporal and routing considerations) effectively unlocks scalability gains, while the PG-BRD-based online stage mitigates congestion and further improves resource utilization.

6.3.2 Evaluation on Interaction Overhead

To quantitatively assess interaction efficiency, we analyze DoI (Fig. 2(c)) and ECoI (Fig. 2(d)). The x-axis (s1–s6) denotes different system configurations (various HU/MU/ES/AP combinations detailed in the caption of the figure), and the y-axis uses a logarithmic scale to capture results across magnitudes. Across all settings, DoI and ECoI remain within the same order of magnitude: FUSION is not always the best in DoI/ECoI, but the gaps with baselines (FUSION_NoPG, FUSION_Random, FUSION_NoST, PurOnline) are rather small. This arises from FUSION’s offline contracting stage, which exposes more candidate SPs and resource options, prompting the PG-BRD online scheduler to explore a larger strategy space, slightly increasing interaction rounds and per-transaction overhead. Importantly, FUSION’s auction and route planning occur offline, adding no extra delay or energy cost to the online stage (DoI/ECoI in Figs. 2(c)–2(d) reflect amortized offline overhead). Combined with SW results (Figs. 2(a)–2(b)), we conclude that FUSION maintains comparable DoI/ECoI to baselines while substantially improving SW through more efficient air-ground resource utilization.

6.3.3 Truthfulness and Individual Rationality

To assess truthfulness and individual rationality, we study the Off-AIC² embedded in FUSION, under a representative setting with 75 HUs, 75 MUs, 12 ESs, and 7 APs. Figs. 2(e) and 2(f) show the utilities of sellers (APs) and buyers (ESs) as functions of their reported asks/bids, while Figs. 2(g) and 2(h) verify individual rationality by comparing true costs/values with payments.

Fig. 2(e) shows four independent market instances, where one AP is randomly selected in each subplot. The horizontal axis denotes the reported ask and the vertical axis the resulting utility (revenue minus true cost), with the blue

dot marking the true ask. As the ask increases, the AP's utility rises while it remains selected, but drops sharply once the ask exceeds its critical region and the contract is lost. In all instances, the utility is maximized near the true ask, indicating that cost misreporting does not improve the seller's payoff. Fig. 2(f) presents a similar analysis for ESs. In each subplot, one ES is selected, with the horizontal axis representing the reported mean bid and the red dot indicating the true valuation. When the bid is below a threshold close to the true value, the ES fails to win and obtains zero utility; once this threshold is crossed, the ES becomes a winner and gains utility, while further bid increases yield negligible gains. Across instances, the best-response region consistently concentrates around the true valuation. The above near-truthful behavior is due to the critical-value-based pricing adopted in the third stage of Off-AIC². A binary-search procedure is used to approximate each participant's critical price, i.e., the lowest effective bid for an ES or the highest effective ask for an AP that guarantees winning. Payments are then determined according to the classical critical-value pricing principle, under which large deviations from true valuations tend to exclude participants from the winner set. Since the allocation problem jointly couples ES-AP matching and route planning and is solved heuristically via eACO-VRP, strict dominant-strategy truthfulness cannot be guaranteed; nevertheless, the empirical results demonstrate consistent near-truthful behavior.

The negative utilities observed in parts of Figs. 2(e) and 2(f) correspond to extreme hypothetical misreports. They arise because utilities are evaluated using true valuations while reported bids/asks are artificially searched over a wide range; such loss-making strategies would not be chosen by rational participants in practice. Figs. 2(g) and 2(h) further confirm individual rationality. For randomly selected winning APs, the total reward determined by Off-AIC² is always no smaller than the corresponding true total cost, and for selected ESs, the true valuation always exceeds the final payment.

7 CONCLUSION AND FUTURE WORK

In this work, we proposed FUSION, a forecasting-driven two-stage framework for service provisioning in air-ground integrated networks with human-machine coexistence. In its offline stage, FUSION leverages Pro-LNN to capture multi-step spatio-temporal dynamics of ES workloads and integrates the predictions into eACO-VRP and Off-AIC² to jointly plan AP routes and design incentive-compatible ES-AP contracts. In its online stage, congestion-aware task scheduling is formulated as an ordinal potential game over heterogeneous HUs, MUs, and SPs (ESs and APs), and addressed via PG-BRD algorithm that obtains a pure-strategy NE while satisfying coverage and capacity constraints. Experiments on both synthetic and real-world datasets show that FUSION consistently achieves higher social welfare and improved resource utilization, while maintaining latency and energy costs comparable to state-of-the-art baselines and preserving individual rationality, budget balance, and near-truthfulness.

Promising future directions include integrating quantum-powered ESs and investigating resource-efficient training and inference of large-scale foundation models in UAV-assisted air-ground networks.

REFERENCES

- [1] L. Kong, J. Tan, J. Huang, G. Chen, S. Wang, X. Jin, P. Zeng, M. Khan, and S. K. Das, "Edge-computing-driven Internet of Things: A survey," *ACM Comput. Surv.*, vol. 55, no. 8, Art. no. 174, pp. 1-41, Dec. 2023.
- [2] Z. Ning, H. Hu, X. Wang, L. Guo, S. Guo, G. Wang, and X. Gao, "Mobile edge computing and machine learning in the Internet of unmanned aerial vehicles: A survey," *ACM Comput. Surv.*, vol. 56, no. 1, Art. no. 13, pp. 1-31, Aug. 2024.
- [3] H. Qi, M. Liwang, X. Wang, L. Li, W. Gong, J. Jin, and Z. Jiao, "Bridge the Present and Future: A Cross-Layer Matching Game in Dynamic Cloud-Aided Mobile Edge Networks," *IEEE Trans. Mobile Comput.*, vol. 23, no. 12, pp. 12522-12523, Dec. 2024.
- [4] G. Sun, Y. Wang, Z. Sun, Q. Wu, J. Kang, D. Niyato, and V. C. M. Leung, "Multi-objective optimization for multi-UAV-assisted mobile edge computing," *IEEE Trans. Mobile Comput.*, vol. 23, no. 12, pp. 14803-14820, 2024.
- [5] M. Hui, J. Chen, L. Yang, L. Lv, H. Jiang, and N. Al-Dhahir, "UAV-assisted mobile edge computing: Optimal design of UAV altitude and task offloading," *IEEE Trans. Wireless Commun.*, vol. 23, no. 10, pp. 13633-13647, Oct. 2024.
- [6] X. Wang, J. Li, J. Wu, L. Guo, and Z. Ning, "Energy efficiency optimization of IRS and UAV-assisted wireless powered edge networks," *IEEE J. Sel. Topics Signal Process.*, vol. 18, no. 7, pp. 1297-1310, 2024.
- [7] J. Xu, H. Yao, R. Zhang, T. Mai, and M. Guizani, "Low latency and accuracy-guaranteed DNN inference for UAV-assisted IoT networks," *IEEE Trans. Cogn. Commun. Netw.*, early access, 2025, doi: 10.1109/TCCN.2025.3542443.
- [8] Y. Li, J. Rao, L. Wang, Y. Xiao, X. Ge, and G. Shi, "Distributed optimization of resource efficiency for federated edge intelligence in AAV-enabled IoT networks," *IEEE Internet Things J.*, vol. 12, no. 8, pp. 9449-9464, Apr. 2025.
- [9] L. Zeng, H. Chen, D. Feng, X. Zhang, and X. Chen, "A3D: Adaptive, accurate, and autonomous navigation for edge-assisted drones," *IEEE/ACM Trans. Netw.*, vol. 32, no. 1, pp. 713-728, Feb. 2024.
- [10] S. Shen, K. Yang, K. Wang, and G. Zhang, "UAV-aided vehicular short-packet communication and edge computing system under time-varying channel," *IEEE Trans. Veh. Technol.*, vol. 72, no. 5, pp. 6625-6638, May 2023.
- [11] J. Tang, K. Fan, S. Yang, A. Liu, N. N. Xiong, H. H. Song, and V. C. M. Leung, "CPDZ: A credibility-aware and privacy-preserving data collection scheme with zero-trust in next-generation crowdsensing networks," *IEEE J. Sel. Areas Commun.*, vol. 43, no. 6, pp. 2183-2199, 2025.
- [12] Y. Ding, K. Li, C. Liu, and K. Li, "A Potential Game Theoretic Approach to Computation Offloading Strategy Optimization in End-Edge-Cloud Computing," *IEEE Trans. Parallel Distrib. Syst.*, vol. 33, no. 6, pp. 1503-1519, Jun. 2022.
- [13] Z. Zhou, L. Pan, and S. Liu, "Potential Game-Based Computation Offloading in Edge Computing With Heterogeneous Edge Servers," *IEEE Trans. Netw. Sci. Eng.*, vol. 12, no. 1, pp. 290-301, Jan. 2025.
- [14] C. Zhang, C. Lee, D. Niyato, and P. Wang, "Auction approaches for resource allocation in wireless systems: A survey," *IEEE Commun. Surveys Tuts.*, vol. 15, no. 3, pp. 1020-1041, 3rd Quart., 2013.
- [15] H. Ren, K. Liu, G. Yan, C. Liu, Y. Li, C. Li, and W. Wu, "Truthful auction mechanisms for dependent task offloading in vehicular edge computing," *IEEE Trans. Mobile Comput.*, vol. 23, no. 12, pp. 14987-15002, Dec. 2024.
- [16] X. Xu, Y. Hu, G. Cui, L. Qi, W. Dou, and Z. Cai, "CADEC: A combinatorial auction for dynamic distributed DNN inference scheduling in edge-cloud networks," *IEEE Trans. Mobile Comput.*, vol. 24, no. 10, pp. 10024-10041, Oct. 2025.
- [17] X. Li, K. Mo, Y. Hou, Z. Li, H. Xu, and N. Guan, "An online auction approach to computing resource allocation in mobile AIGC networks," *IEEE Internet Things J.*, vol. 12, no. 8, pp. 11182-11193, Apr. 2025.
- [18] R. Lu, W. Zhang, Y. Wang, Q. Li, X. Zhong, H. Yang, and D. Wang, "Auction-based cluster federated learning in mobile edge computing systems," *IEEE Trans. Parallel Distrib. Syst.*, vol. 34, no. 4, pp. 1145-1158, Apr. 2023.
- [19] C.-Y. Hsieh, Y. Ren, and J.-C. Chen, "Edge-cloud offloading: Knapsack PG in 5G multi-access edge computing," *IEEE Trans. Wireless Commun.*, vol. 22, no. 11, pp. 7158-7171, Nov. 2023.
- [20] L. Wu, P. Sun, Z. Wang, Y. Li, and Y. Yang, "Computation offloading in multi-cell networks with collaborative edge-cloud computing: A game theoretic approach," *IEEE Trans. Mobile Comput.*, vol. 23, no. 3, pp. 2093-2106, Mar. 2024.
- [21] A. R. Hossain, W. Liu, and N. Ansari, "AI-native end-to-end network slicing for next-generation mission-critical services," *IEEE Trans. Cogn. Commun. Netw.*, vol. 11, no. 1, pp. 48-58, 2025.
- [22] S. Wu, M. Liwang, D. Wang, X. Wang, C. Wu, J. Tang, L. Li, and X. Xia, "Effective two-stage double auction for dynamic resource provision over edge networks via discovering the power of overbooking," *IEEE Trans. Serv. Comput.*, early access, pp. 1-13, 2025.
- [23] M. Chahine, R. Hasani, P. Kao, A. Ray, R. Shubert, M. Lechner, A. Amini, and D. Rus, "Robust flight navigation out of distribution with liquid neural networks," *Sci. Robot.*, vol. 8, no. 77, Art. ead8892, 2023.
- [24] J. L. Ba, J. R. Kiro, and G. E. Hinton, "Layer normalization," arXiv preprint arXiv:1607.06450, 2016.
- [25] H. Qi, M. Liwang, X. Wang, L. Fu, Y. Hong, L. Li, and Z. Cheng, "Accelerating stable matching between workers and spatial-temporal tasks for dynamic MCS: A stagewise service trading approach," *IEEE Trans. Mobile Comput.*, early access, pp. 1-16, 2025, doi: 10.1109/TMC.2025.3610915.
- [26] J. Li, Y. Xiong, and J. She, "UAV path planning for target coverage task in dynamic environment," *IEEE Internet Things J.*, vol. 10, no. 20, pp. 17734-17745, 2023.
- [27] S. Spana, L. Du and Y. Yin, "Strategic Information Perturbation for an Online In-Vehicle Coordinated Routing Mechanism for Connected Vehicles Under Mixed-Strategy Congestion Game," *IEEE Trans. Intell. Transp. Syst.*, vol. 23, no. 5, pp. 4541-4555, May 2022.

- [28] S. Hochreiter and J. Schmidhuber, "Long short-term memory," *Neural Comput.*, vol. 9, no. 8, pp. 1735-1780, Nov. 1997, doi: 10.1162/neco.1997.9.8.1735.
- [29] A. Vaswani, N. Shazeer, N. Parmar, J. Uszkoreit, L. Jones, A. N. Gomez, L. Kaiser, and I. Polosukhin, "Attention is all you need," in *Proc. Adv. Neural Inf. Process. Syst. (NeurIPS)*, 2017.
- [30] H. Qi, M. Liwang, S. Hosseinalipour, L. Fu, S. Zou, and W. Ni, "Future resource bank for ISAC: Achieving fast and stable win-win matching for both individuals and coalitions," *IEEE J. Sel. Areas Commun.*, early access, 2025, doi: 10.1109/JSAC.2025.3608114.
- [31] Z. Yang, S. Bi, and Y.-J. A. Zhang, "Dynamic offloading and trajectory control for UAV-enabled mobile edge computing system with energy harvesting devices," *IEEE Trans. Wireless Commun.*, vol. 21, no. 12, pp. 10515-10528, 2022.
- [32] 5G Americas, "New services & applications with 5G ultra-reliable low latency communications," White Paper, Nov. 2018.
- [33] 3GPP, "5G; Study on scenarios and requirements for next generation access technologies," 3GPP TR 38.913, ver. 17.0.0, Release 17, 2022.
- [34] A. Trindade, "ElectricityLoadDiagrams20112014," UCI Mach. Learn. Repository, 2015. [Online]. Available: <https://doi.org/10.24432/C58C86>.

APPENDIX A KEY NOTATIONS

Key notations in this paper are summarized in Table 5.

APPENDIX B DETAILED OF OFFLINE STAGE

B.1 Detailed Pro-LNN Architecture and Training Procedure

In this section, we provide the detailed update equations and training procedure of the proposed Pro-LNN predictor used in Off-AIC².

Step 1. Stable liquid cell (line 7, Alg. 4): At the core of Pro-LNN is a stable liquid cell that updates a hidden state $\mathbf{h}_i^{(\nu)} \in \mathbb{R}^d$ given the current input $\mathbf{z}_i^{(\nu)}$ and the previous state. Concretely, we first compute neuron-wise time constants and a pre-activation: $\tau^{(\nu)} = \text{softplus}(W_\tau[\mathbf{z}_i^{(\nu)}, \mathbf{h}_i^{(\nu)}]) + \tau_{\min}$ and $\tilde{\mathbf{u}}^{(\nu)} = W_h \mathbf{h}_i^{(\nu)} + W_x \mathbf{z}_i^{(\nu)} + \mathbf{b}$, where W_τ, W_h, W_x and \mathbf{b} are trainable, and $\tau_{\min} > 0$ enforces strictly positive time scales (we also clamp $\tau^{(\nu)}$ to $[\tau_{\min}, \tau_{\max}]$ for numerical stability). The effective update rate is then $\alpha^{(\nu)} = \text{clip}\left(\frac{\Delta\nu}{\tau^{(\nu)}}, \alpha_{\min}, \alpha_{\max}\right)$, with a fixed $\Delta\nu$ (one trading interval in our implementation) and small constants $0 < \alpha_{\min} \leq \alpha_{\max} < 1$. We then apply a lightweight layer normalization and non-linearity, $\tilde{\mathbf{h}}_i^{(\nu)} = \tanh(\text{LN}(\tilde{\mathbf{u}}^{(\nu)}))$, and update the hidden state as

$$\mathbf{h}_i^{(\nu+1)} = (1 - \alpha^{(\nu)}) \odot \mathbf{h}_i^{(\nu)} + \alpha^{(\nu)} \odot \tilde{\mathbf{h}}_i^{(\nu)} + \gamma \tanh(\text{LN}(\mathbf{h}_i^{(\nu)})), \quad (24)$$

where γ is a small residual scaling factor and \odot denotes element-wise multiplication. This leaky-integrator update

blends exponential memory decay with input-driven state injection, while the neuron-wise $\tau^{(\nu)}$ allow different neurons to operate at different effective time scales.

Notation. For clarity, all nonlinear operators in the above update are applied element-wise unless otherwise stated. Specifically, $\text{softplus}(\cdot)$ denotes the standard softplus activation $\text{softplus}(x) = \log(1 + e^x)$, $\text{clip}(x, a, b)$ clips each element of x into the interval $[a, b]$, $\text{LN}(\cdot)$ denotes layer normalization [24], and $\text{LiquidCell}(\mathbf{z}_i^{(\nu)}, \mathbf{h}_i^{(\nu)})$ is a shorthand for one step of the stable liquid update in Step 1 (using the time-constant gating and residual integration described above).

Step 2. Historical encoding (lines 4-7, Alg. 4): Given the latest L observations of ES s_i up to trading round ν , Pro-LNN encodes the history by iteratively applying the liquid cell: $\mathbf{h}_i^{(\nu-L+1)} \leftarrow \text{LiquidCell}(\mathbf{z}_i^{(\nu-L+1)}, \mathbf{0}), \dots, \mathbf{h}_i^{(\nu)} \leftarrow \text{LiquidCell}(\mathbf{z}_i^{(\nu)}, \mathbf{h}_i^{(\nu-1)})$.

This exponential-style integration naturally adapts memory decay and information injection under irregular or noisy trajectories.

Step 3. Multi-horizon readout and consistency (lines 8-17, Alg. 4): After encoding the history, a shallow MLP readout maps the final hidden state to an H -step forecast:

$$\hat{\mathbf{n}}_i^{(1:H)} = \text{Readout}(\mathbf{h}_i^{(\nu)}) = [\hat{N}_i^{\text{Dem},(\nu+1)}, \dots, \hat{N}_i^{\text{Dem},(\nu+H)}], \quad (25)$$

where $\text{Readout}(\cdot)$ denotes a lightweight fully connected network that maps the d -dimensional hidden state to an H -dimensional prediction vector. The base training loss is the mean squared error (MSE) over the H horizons. To further improve stability for long horizons, we optionally add a *multi-step consistency* objective: starting from a history window, we

TABLE 5
Key notations

Notation	Explanation
$\mathcal{S}, \mathcal{U}^H, \mathcal{U}^M, \mathcal{V}$	Sets of edge servers (ESs), human users (HUs), machine users (MUs), and air-ground providers (APs)
s_i, u_m^H, u_n^M, v_k	The i -th ES, the m -th HU, the n -th MU, and the k -th AP
$N_i^{\text{Dem},(\nu)}, \hat{N}_i^{\text{Dem},(\nu+h)}$	Actual and LNN-predicted task demand of ES s_i at trading rounds ν and $\nu+h$
$l_i^E, l_m^H, l_n^M, l_k^A$	3D locations of ES s_i , HU u_m^H , MU u_n^M , and the dispatching vehicle of AP v_k
r_m^H, r_n^M, r_j	Computation workload (CPU cycles) of HU u_m^H , MU u_n^M , and generic SD u_j^{On}
d_m^H, d_n^M, d_j	Input data size (bits) of HU tasks, MU tasks, and generic SD tasks
$f_i^E, f_i^{\text{On}}, f_m^{\text{H,loc}}, f_n^{\text{M,loc}}, f_k^A$	Computing capabilities of ES s_i , online SP s_i^{On} , local HU/MU devices, and UAVs dispatched by AP v_k
$e_m^{\text{H,tx}}, e_n^{\text{M,tx}}$	Uplink transmit power of HU u_m^H and MU u_n^M
e_i^E	Local computing energy consumption of ES s_i
$e_k^{\text{comp}}, e_k^{\text{move}}, e_k^{\text{fly}}$	Energy consumption of AP v_k for computation, ground movement, and UAV flight
$\tau_n^{\text{ddl}}, \tau_j^{\text{ddl}}$	Task deadline of MU u_n^M in offline stage and latency deadline of SD u_j^{On} in online stage
C_k^A	Total number of UAVs carried by AP v_k
$N_{i,k}^{\text{Trad}}$	Quantity of traded computing resources between ES s_i and AP v_k in an offline contract
$x_{i,k}^{\text{OH}}, \mathbf{X}$	Binary offline assignment between ES s_i and AP v_k ; \mathbf{X} collects all $x_{i,k}^{\text{OH}}$
$p_{i,k}^{\text{ES}}, p_{i,k}^{\text{ES}}, \tilde{p}_i$	Payment from ES s_i to AP v_k , reward received by v_k , and historical average user service price at s_i
$U_i^{\text{ES,OH}}, U_k^A, U^{\text{Auc}}$	Utility of ES s_i , utility of AP v_k , and utility of the auctioneer in offline stage
U^{SW}	Total SW of the offline auction market (sum of utilities of ESs, APs, and auctioneer)
$\mathcal{G}_k(\mathcal{N}_k, \mathcal{E}_k), \mathbb{K}$	Directed complete graph and ant set used by eACO-VRP for routing AP v_k
$\varphi_{r,s}, \eta_{r,s}, p_{n_r \rightarrow n_s}^c$	Pheromone level, distance, and transition probability on edge (n_r, n_s) in eACO-VRP
$\mathcal{S}^{\text{On}}, \mathcal{U}^{\text{On}}, \mathcal{H}, \mathcal{A}$	Sets of online service providers (SPs), service demanders (SDs), HUs and MUs in online stage
$x_j^{\text{On}}, x_{j,i}^{\text{On}}, \mathbf{x}_j$	Indicator of local execution, indicator of scheduling SD u_j^{On} to SP s_i^{On} , and the scheduling vector of SD u_j^{On}
$y_i, \mathbf{x}_i, n_i(\boldsymbol{\pi})$	Effective congestion load, aggregate computing load, and number of associated SDs at SP s_i^{On} under profile $\boldsymbol{\pi}$
$t_{j,i}^{\text{comp}}, t_{j,i}^{\text{tx}}, T_{j,i}^{\text{edge}}$	Computation delay, uplink transmission delay, and total edge-side latency of SD u_j^{On} at SP s_i^{On}
$S_j(\hat{i}), \kappa_j, \theta_{j,i}, \tau_i(y)$	Non-congestion benefit term, congestion sensitivity, load factor, and congestion function at SP s_i^{On}
$K_i(\mathbf{x}_i), C_i$	Computation/operation cost function and maximum computing capacity of SP s_i^{On}
$\boldsymbol{\pi}, \Phi(\boldsymbol{\pi}), \mathcal{F}^{(I)}, \mathcal{F}^{(II)}$	Joint scheduling profile, ordinal potential function, and optimization problems in offline stage and online stage

Algorithm 4: Pro-LNN

Input: Training sequences $\{\mathbf{z}_i^{(1:T)}\}$; history length L ; horizon H ; learning rate η ; consistency depth K

Output: Predicted sequences $\{\hat{N}_i^{\text{Dem},(\nu+1:\nu+H)}\}$

- 1 Initialize liquid-cell and readout parameters θ ;
- 2 **while** not converged **do**
- 3 Sample a mini-batch \mathcal{B} of training windows from \mathcal{D} ;
- 4 **for** each window $(\mathbf{z}_i^{(\nu-L+1:\nu)}, N_i^{\text{Dem},(\nu+1:\nu+H)}) \in \mathcal{B}$ **do**
- 5 Set hidden state $\mathbf{h}_i \leftarrow \mathbf{0}$;
- 6 **for** $k = \nu - L + 1$ **to** ν **do**
- 7 $\mathbf{h}_i \leftarrow \text{LiquidCell}(\mathbf{z}_i^{(k)}, \mathbf{h}_i)$;
- 8 **(Base H -step forecast)**
- 9 $\hat{\mathbf{n}}_i^{(1:H)} \leftarrow \text{Readout}(\mathbf{h}_i)$;
- 10 $\mathcal{L}_i \leftarrow \frac{1}{H} \sum_{h=1}^H (\hat{n}_i^{(h)} - N_i^{\text{Dem},(\nu+h)})^2$;
- 11 **if** $K > 0$ **then**
- 12 Construct a history window \mathbf{y}_i from $\{\mathbf{z}_i^{(\nu-L+1)}, \dots, \mathbf{z}_i^{(\nu)}\}$;
- 13 **for** $k = 1$ **to** K **do**
- 14 $\hat{\mathbf{n}}_i^{(1:H)} \leftarrow f_\theta(\mathbf{y}_i)$;
- 15 $\mathcal{L}_i \leftarrow \mathcal{L}_i + (\hat{n}_i^{(1)} - N_i^{\text{Dem},(\nu+k)})^2$;
- 16 Update \mathbf{y}_i by discarding the oldest step and appending $\hat{n}_i^{(1)}$ as the newest demand;
- 17 $\mathcal{L}_i \leftarrow \mathcal{L}_i / (H + K)$;
- 18 Aggregate loss $\mathcal{L} \leftarrow \frac{1}{|\mathcal{B}|} \sum_{i \in \mathcal{B}} \mathcal{L}_i + \lambda \Omega(\theta)$;
- 19 Update parameters $\theta \leftarrow \theta - \eta \nabla_\theta \mathcal{L}$;

repeatedly roll the model forward in closed loop by feeding its own one-step predictions back into the window, and penalize the mismatch at each rolled-out step.

Step 4. Inference and integration (line 9, Alg. 4): At inference, Pro-LNN takes, for each ES s_i , the latest L observations $\{\mathbf{z}_i^{(\nu-L+1)}, \dots, \mathbf{z}_i^{(\nu)}\}$, encodes them via the liquid cell into $\mathbf{h}_i^{(\nu)}$, and applies the readout to obtain an H -step forecast $\{\hat{N}_i^{\text{Dem},(\nu+1)}, \dots, \hat{N}_i^{\text{Dem},(\nu+H)}\}$. These predictions are computed in the offline stage before each trading round and then fed into: (i) the eACO-VRP module for time-window-aware ES recommendation and AP route pre-planning, and (ii) the auction module for ES-AP contract design. Since Pro-LNN runs offline, its wall-clock inference latency does not affect the real-time trading between SDs and SPs, while its compact footprint and robustness to noisy inputs make it well suited for deployment on edge and near-edge computing platforms.

B.2 Economic Properties of Off-AIC²

Here, we discuss the fundamental properties that underpin the design of auction in offline stage [14], [22].

Proposition 1. (Individual Rationality) *An auction is said to be individually rational if the payment made by any winning ES (to its matched AP) does not exceed its bid, and the revenue obtained by any winning AP is no less than its asked price.*

Proposition 2. (Near-Truthfulness) *An auction mechanism is said to be near-truthful if every ES and AP maximizes, or almost maximizes, its utility by reporting its true private valuation. In particular, for any fixed bids and asks of the other participants, no single ES or AP can increase its utility by more than a small margin through unilaterally misreporting its bid or ask. In this sense, truthful reporting remains an empirically near-optimal strategy, and large deviations from true valuations are not beneficial.*

Proposition 3. (Budget Balance) *An auction satisfies budget balance if the total payment collected from all winning ESs is no less than the total payment made to all winning APs.*

Proposition 4. *All winning ESs and APs obtained from Off-AIC² are individually rational during the offline stage.*

The proposed offline stage of FUSION is shown to meet all the above properties, with detailed theoretical analysis as follow.

Proof. The individual rationality of Off-AIC² is guaranteed by the core design of its allocation (Step 2) and pricing (Step 3) procedures in Alg. 2, under the single-parameter assumption that each ES s_i has a per-unit valuation and each AP v_k has a per-unit cost.

(i) **ES side (buyers).** We first consider ES buyers s_i .

- *Allocation in Step 2:* For each AP v_k , the candidate ES set is constructed as

$$\mathcal{C}_k = \{i \in \mathcal{U}^{\text{free}} \mid U_{i,k} > 0 \wedge \text{bid}_{i,k} \geq \overline{\text{bid}}_i\}, \quad (26)$$

where $U_{i,k} = \text{bid}_{i,k} - \text{ask}_k$ denotes the surplus of matching ES s_i with AP v_k . Hence, if ES s_i is eventually matched (i.e., there exists some k such that $x_{i,k}^{\text{Off}} = 1$), the corresponding pair (s_i, v_k) must satisfy

$$U_{i,k} = \text{bid}_{i,k} - \text{ask}_k > 0, \quad \text{bid}_{i,k} \geq \overline{\text{bid}}_i. \quad (27)$$

Under truthful bidding, $\text{bid}_{i,k}$ equals s_i 's true per-unit valuation for the contracted service. Therefore, already at the allocation stage, every winning ES enjoys a strictly positive surplus margin between its valuation and the AP's ask.

- *Pricing in Step 3:* In Step 3, for each winning ES s_i with $\sum_k x_{i,k}^{\text{Off}} = 1$, Off-AIC² treats its effective bid as a variable and performs a monotone binary search over an interval of the form

$$p_i^{\text{b}*} \in [\underline{b}_i, \overline{\text{bid}}_i], \quad (28)$$

where $\overline{\text{bid}}_i$ is s_i 's reference bid (coinciding with its true valuation when truthful) and \underline{b}_i is a market-wide lower bound. The binary search stops at the *minimal* critical payment that keeps s_i in the winning set when Step 2 is re-executed. By construction, we have

$$p_i^{\text{b}*} \leq \overline{\text{bid}}_i. \quad (29)$$

Moreover, for the realized winning pair (i, k) we also have $\text{bid}_{i,k} \geq \overline{\text{bid}}_i$. Combining these relations yields

$$\text{bid}_{i,k} \geq \overline{\text{bid}}_i \geq p_i^{\text{b}*}. \quad (30)$$

Under truthful bidding, $\text{bid}_{i,k}$ is ES s_i 's true valuation, while $p_i^{\text{b}*}$ is its actual per-unit payment in Off-AIC². Hence the ex-post utility of s_i in the offline stage satisfies

$$u_i^{\text{ES}} = (\text{valuation}) - (\text{payment}) \geq \text{bid}_{i,k} - p_i^{\text{b}*} \geq 0, \quad (31)$$

which proves individual rationality for all winning ESs.

(ii) **AP side (sellers).** We now turn to AP sellers v_k .

- *Allocation in Step 2:* In Step 2, APs only serve ESs that yield strictly positive surplus, and they are protected by capacity constraints. Specifically, v_k may serve ES s_i only if $U_{i,k} = \text{bid}_{i,k} - \text{ask}_k > 0$, and the matching obeys

$$\sum_i x_{i,k}^{\text{Off}} N_i^{\text{Dem}} \leq C_k^{\text{A}}. \quad (32)$$

Under truthful reporting, ask_k equals v_k 's true per-unit cost. Thus each winning AP only accepts contracts where the buyer-side valuation exceeds its cost, ensuring a nonnegative surplus margin at the allocation stage.

• *Pricing in Step 3:* In Step 3, for each winning AP v_k with $\sum_i x_{i,k}^{\text{Off}} \geq 1$, Off-AIC² performs a monotone binary search over an interval

$$r_k^{\text{S*}} \in [\text{ask}_k, \bar{r}_k], \quad (33)$$

where ask_k is its own ask (true cost when truthful) and \bar{r}_k is a market-determined upper bound. The search stops at the *maximal* critical reward that still keeps v_k in the winning set when Step 2 is rerun. Consequently, we have

$$r_k^{\text{S*}} \geq \text{ask}_k. \quad (34)$$

Under truthful reporting, ask_k is v_k 's true per-unit cost, and $r_k^{\text{S*}}$ is the actual per-unit reward it receives. Hence the ex-post utility of v_k in the offline stage is

$$u_k^{\text{AP}} = (r_k^{\text{S*}} - \text{ask}_k) \cdot \left(\sum_i x_{i,k}^{\text{Off}} N_i^{\text{Dem}} \right) \geq 0. \quad (35)$$

In summary, by construction of the candidate sets and critical-value pricing, every winning ES pays no more than its valuation, and every winning AP receives no less than its cost. Therefore, Off-AIC² is individually rational for both ESs and APs in the offline stage. ■

Proposition 5 (Near-truthfulness of Off-AIC²). *Off-AIC² mechanism is near-truthful for both ESs and APs in the offline stage.*

Proof. At a high level, Off-AIC² follows the same structural design as classical truthful single-parameter auctions: on both the ES side and the AP side, it combines a (approximately) monotone allocation rule with critical-value-like payments obtained via binary search. In fully monotone settings, such a combination is sufficient for dominant-strategy incentive compatibility; in our case, the presence of route planning via eACO-VRP makes the allocation only *approximately* monotone, and therefore we obtain approximate (rather than exact) truthfulness.

(i) ES side (buyers). Fix any ES s_i and treat all other bids and asks as given. Under the single-parameter simplification, s_i reports a single per-unit bid b_i , which induces its bid row $\text{bid}_{i,k} = b_i$ and average bid $\bar{\text{bid}}_i = b_i$.

Approximate monotone allocation (Steps 1 & 2). In Step 1, ESs are sorted in nonincreasing order of $\bar{\text{bid}}_i = b_i$. Increasing b_i can only move s_i upward in this list; it never pushes s_i to a worse rank. Since Off-AIC² only considers the top- I^* ESs, once s_i belongs to the top- I^* at some bid b_i , it remains in the top- I^* for any higher bid $b'_i > b_i$.

In Step 2, a necessary condition for s_i to be matched is that it lies in the top- I^* ESs and that there exists an AP v_k such that

$$U_{i,k}^{\text{Off}} = \text{bid}_{i,k} - \text{ask}_k = b_i - \text{ask}_k > 0, \quad \bar{\text{bid}}_i \geq \text{ask}_k. \quad (36)$$

If we ignore the internal randomness and heuristic nature of eACO-VRP, raising b_i strictly increases all $U_{i,k}^{\text{Off}}$, making s_i (weakly) more attractive and therefore easier to be selected. In practice, the eACO-VRP-based matching can occasionally break strict monotonicity because ES-AP matching and route planning are coupled in a combinatorial way; however, for a fixed tie-breaking rule and fixed routes of other APs, the allocation rule behaves *approximately* monotone in b_i : once s_i is selected at some bid level, it typically remains selected for any sufficiently close higher bid $b'_i > b_i$.

Critical-value-like payment (Step 3). In Step 3, for each winning ES s_i (with $\sum_k x_{i,k}^{\text{Off}} = 1$), Off-AIC² treats its

effective bid as a variable and performs a monotone binary search over an interval

$$b_i^{\text{eff}} \in [\underline{b}_i, \bar{\text{bid}}_i], \quad (37)$$

repeatedly re-running Step 2 to check whether s_i would still be selected. The search stops at the smallest bid at which s_i remains a winner, and the resulting value is taken as its payment $p_i^{\text{b*}}$. When the allocation subroutine is exactly monotone, $p_i^{\text{b*}}$ coincides with the classical *critical value* and yields exact dominant-strategy truthfulness. With eACO-VRP, the binary-search procedure still emulates such a critical value and produces a payment that depends only weakly on s_i 's own report as long as b_i stays in a small neighborhood above $p_i^{\text{b*}}$. Our numerical results (Fig. 2(f)) confirm that s_i 's realized utility curve is single-peaked around its true valuation, and deviations from truthful bidding only bring marginal utility gains, if any. Hence truthful bidding is a locally optimal strategy and nearly utility-maximizing for ESs.

(ii) AP side (sellers). Now fix an AP v_k and consider its per-unit ask a_k , treating all ES bids and other APs' asks as fixed. Under the single-parameter simplification, a_k is v_k 's single strategic parameter.

Approximate monotone allocation (Steps 1 & 2). In Step 1, APs are sorted in nondecreasing order of $\text{ask}_k = a_k$. Lowering a_k can only move v_k upward in this list, never downward. Since Off-AIC² only considers the top- K^* APs, once v_k lies in the top- K^* at some ask a_k , it remains in the top- K^* for any lower ask $a'_k < a_k$.

In Step 2, v_k 's attractiveness to ESs is determined by the surplus terms

$$U_{i,k}^{\text{Off}} = \text{bid}_{i,k} - a_k. \quad (38)$$

Lowering a_k strictly increases all $U_{i,k}^{\text{Off}}$, making v_k more competitive. With a fixed eACO-VRP configuration, this behavior again yields an allocation rule that is approximately monotone in $-a_k$: once v_k is selected at some ask a_k , it tends to remain selected for any sufficiently close lower ask $a'_k < a_k$, except for rare non-monotone cases introduced by heuristic route decisions.

Critical-reward-like payment (Step 3). For each winning AP v_k (with $\sum_i x_{i,k}^{\text{Off}} \geq 1$), Step 3 treats its effective ask as a variable and performs a binary search over

$$a_k^{\text{eff}} \in [\text{ask}_{K^*+1}, \text{ask}_k], \quad (39)$$

re-running Step 2 to check whether v_k would still be selected. The search terminates at the largest ask at which v_k remains a winner, and the corresponding reward $r_k^{\text{S*}}$ plays the role of a critical ask. When the allocation is exactly monotone, this would give a classical critical payment; with eACO-VRP, $r_k^{\text{S*}}$ still behaves as a critical-reward approximation. Empirically (Fig. 2(e)), v_k 's realized utility as a function of a_k exhibits a clear peak near its true ask, and over-reporting beyond that region mostly increases the risk of losing the contract without improving utility. Thus, truthful asking is again a locally best or near-best strategy for APs.

Putting the buyer and seller sides together, Off-AIC² combines (i) an allocation rule that is monotone up to small perturbations due to the heuristic eACO-VRP subroutine, and (ii) payments and rewards that closely emulate critical values via binary search. According to our definition of approximate truthfulness, this implies that, for both ESs and APs, truthful reporting is a (local) utility-maximizing strategy and any unilateral deviation from the true valuation changes the

utility by at most a small margin, as also corroborated by the numerical evidence in Figs. 2(e)–2(f). Therefore, Off-AIC² is near-truthful for both ESs and APs in the offline stage. ■

Proposition 6. *Off-AIC² satisfies the (weak) budget-balance property in the offline stage.*

Proof. To verify budget balance, it suffices to show that the auctioneer’s utility in the offline stage,

$$U^P = \sum_{s_i \in \mathcal{S}} \sum_{v_k \in \mathcal{V}} x_{i,k}^{\text{Off}} N_{i,k}^{\text{Trad}} (p_{i,k}^{\text{ES}} - r_{i,k}^{\text{ES}}), \quad (40)$$

is nonnegative, i.e., $U^P \geq 0$. Since $N_{i,k}^{\text{Trad}} \geq 0$ and $x_{i,k}^{\text{Off}} \in \{0, 1\}$, this reduces to proving that for every active trading pair (i, k) with $x_{i,k}^{\text{Off}} = 1$,

$$p_{i,k}^{\text{ES}} - r_{i,k}^{\text{ES}} \geq 0. \quad (41)$$

(i) Phase 1 (pivotal-rank selection). In Step 1 of Alg. 2, ESs are sorted in nonincreasing order of their average bids $\overline{\text{bid}}_i$, and APs are sorted in nondecreasing order of their asks ask_k . The pivotal ranks (I^*, K^*) are chosen such that

$$\overline{\text{bid}}_{I^*} \geq \text{ask}_{K^*}, \quad \sum_{k=1}^{K^*} C_k^A \geq \sum_{i=1}^{I^*} N_i^{\text{Dem}}. \quad (42)$$

Alg. 2 only considers the top- I^* ESs and top- K^* APs for matching. Hence, for any winning pair (i, k) with $x_{i,k}^{\text{Off}} = 1$, we have

$$\text{bid}_{i,k} \geq \overline{\text{bid}}_{I^*} \geq \text{ask}_{K^*} \geq \text{ask}_k. \quad (43)$$

Equation (43) shows that, for each matched pair (i, k) , there exists a nonempty price band

$$\{(p, r) \mid \text{ask}_k \leq r \leq p \leq \text{bid}_{i,k}\} \quad (44)$$

in which both ES s_i and AP v_k obtain nonnegative utilities and the auctioneer’s per-unit margin $p - r$ is nonnegative.

(ii) Phase 3 (critical pricing). Step 3 of Alg. 2 determines the actual payments within this feasible band using critical-value binary searches:

- *Buyer side (ESs):* For each winning ES s_i with $\sum_k x_{i,k}^{\text{Off}} = 1$, the payment $p_i^{\text{b}*}$ is obtained via a monotone binary search on its effective bid parameter. The search interval is chosen inside the buyer side of the surplus-feasible band in (43), and the algorithm stops at the minimum critical bid that keeps s_i in the winning set when Step 2 is re-executed. Thus, for any matched pair (i, k) ,

$$p_{i,k}^{\text{ES}} = p_i^{\text{b}*} \leq \text{bid}_{i,k}. \quad (45)$$

- *Seller side (APs):* Similarly, for each winning AP v_k with $\sum_i x_{i,k}^{\text{Off}} \geq 1$, the reward $r_k^{\text{s}*}$ is obtained via a monotone binary search on its effective ask parameter. The search interval is chosen inside the seller side of the band in (43), and the algorithm stops at the maximum critical ask that keeps v_k in the winning set. Hence, for any matched pair (i, k) ,

$$r_{i,k}^{\text{ES}} = r_k^{\text{s}*} \geq \text{ask}_k. \quad (46)$$

Because both searches are confined to the common surplus-feasible band identified in (43), off-AIC² always chooses prices satisfying

$$\text{ask}_k \leq r_{i,k}^{\text{ES}} \leq p_{i,k}^{\text{ES}} \leq \text{bid}_{i,k}, \quad \forall (i, k) \text{ with } x_{i,k}^{\text{Off}} = 1. \quad (47)$$

In particular, we obtain

$$p_{i,k}^{\text{ES}} - r_{i,k}^{\text{ES}} \geq 0 \quad \forall (i, k) \text{ with } x_{i,k}^{\text{Off}} = 1. \quad (48)$$

(iii) Concluding budget balance. Therefore, each active trading pair contributes a nonnegative margin

$$x_{i,k}^{\text{Off}} N_{i,k}^{\text{Trad}} (p_{i,k}^{\text{ES}} - r_{i,k}^{\text{ES}}) \geq 0, \quad (49)$$

while unmatched pairs contribute zero. Summing over all ES–AP pairs gives

$$U^P = \sum_{i,k} x_{i,k}^{\text{Off}} N_{i,k}^{\text{Trad}} (p_{i,k}^{\text{ES}} - r_{i,k}^{\text{ES}}) \geq 0, \quad (50)$$

which completes the proof that Off-AIC² is (weakly) budget balanced in the offline stage. ■

APPENDIX C

PROPERTIES OF THE ORDINAL POTENTIAL

To turn the above game formulation into a practical distributed scheduling mechanism, we need a global scalar function whose improvement is aligned with individual SD incentives. In particular, if $\Phi(\pi)$ acts as an *ordinal potential*, then any unilateral utility-improving move by an SD strictly increases $\Phi(\pi)$. This property is exactly what allows simple asynchronous better-/best-response dynamics to converge to a pure-strategy NE with provable guarantees and low online complexity. We therefore establish that the function $\Phi(\pi)$ in (21) is an ordinal potential for the online game under soft-deadline valuations.

The proof follows a standard single-user deviation argument and relies on three ingredients: (i) separability of the non-congestion terms $S_j(\cdot)$, (ii) an integral–pointwise comparison that links the *pointwise* congestion penalty in user utilities with the *integrated* congestion cost in $\Phi(\pi)$, and (iii) monotonicity and convexity of the SP-side cost $K_i(\cdot)$. Full details are deferred to Appendices D.3–D.7.

Proposition 7 (Ordinal potential). *Consider the unified utilities in (19) with soft-deadline MUs and the potential $\Phi(\pi)$ in (21). For any SD u_j^{On} and any unilateral deviation $\pi_j = \mathbf{i} \rightarrow \mathbf{i}'$, if $U_{j,\mathbf{i}'} - U_{j,\mathbf{i}} > 0$, then $\Phi(\pi_{-\mathbf{j},\mathbf{i}'}) - \Phi(\pi_{-\mathbf{j},\mathbf{i}}) > 0$. Hence, $\Phi(\pi)$ is an ordinal potential for the considered game [13].*

Since each SD possesses a finite action set, any sequence of unilateral best-response (or better-response) updates generates a strictly increasing trajectory of the potential function $\Phi(\pi)$ and therefore converges in finitely many iterations to a pure-strategy NE. Equivalently, every local maximizer of $\Phi(\pi)$ corresponds to a pure-strategy NE of the online scheduling game. A formal proof of this finite-improvement property is provided in Appx. D.8.

APPENDIX D

PROOF DETAILS FOR THE ORDINAL POTENTIAL AND PG-BRD

This appendix collects the main technical ingredients behind the ordinal-potential formulation in the online stage and the design of PG-BRD. We have: (i) rewrite the model using a global assignment matrix, (ii) relate pointwise congestion penalties to integrated congestion via a simple sandwich inequality, (iii) characterize single-user deviations and the linearized soft-deadline utility, (iv) prove the ordinal-potential property and finite-improvement path (FIP), and (v) clarify why monetary payments are excluded from the potential.

D.1 Matrix Formulation Based on the Global Assignment Matrix

For some of the theoretical arguments and for vectorized implementations, it is convenient to represent the joint offloading profile by a single global matrix.

Global assignment matrix. Define

$$\mathbf{X} \in \{0, 1\}^{|\mathcal{U}^{\text{On}}| \times (1 + |\mathcal{S}^{\text{On}}|)} \quad (51)$$

by stacking each SD's binary decision vector $\mathbf{X}_j^{\text{On}} = (x_{j,1}^{\text{On}}, x_{j,1}^{\text{On}}, \dots, x_{j,|\mathcal{S}^{\text{On}}|}^{\text{On}})$. The $(j, 0)$ -th entry corresponds to local execution ($\pi_j = 0$), and the (j, i) -th entry corresponds to offloading to s_i^{On} ($\pi_j = i$). Under the one-hot per-row constraint $\sum_i x_{j,i}^{\text{On}} + x_j^{\text{On}} = 1$, \mathbf{X} and $\boldsymbol{\pi}$ are equivalent representations.

Aggregates in matrix form. Using \mathbf{X} , the effective congestion load and physical workload at SP s_i^{On} are

$$y_i(\mathbf{X}) = \sum_{j \in \mathcal{U}^{\text{On}}} \gamma_{j,i} x_{j,i}^{\text{On}}, \quad \mathbf{x}_i(\mathbf{X}) = \sum_{j \in \mathcal{U}^{\text{On}}} r_j x_{j,i}^{\text{On}}. \quad (52)$$

These expressions are directly usable in optimization-based or vectorized implementations of PG-BRD.

Potential in matrix form. Substituting (52) into the potential in (21), we obtain the equivalent representation

$$\begin{aligned} \Phi(\mathbf{X}) &= \sum_{j \in \mathcal{U}^{\text{On}}} \sum_{i \in \mathcal{S}^{\text{On}}} S_j(i) x_{j,i}^{\text{On}} - \sum_{i \in \mathcal{S}^{\text{On}}} \int_0^{y_i(\mathbf{X})} \tau_i(z) dz \\ &\quad - \sum_{i \in \mathcal{S}^{\text{On}}} K_i(\mathbf{x}_i(\mathbf{X})), \end{aligned} \quad (53)$$

which coincides with $\Phi(\boldsymbol{\pi})$ whenever each row of \mathbf{X} has exactly one nonzero entry. In this form, $\Phi(\mathbf{X})$ decomposes into: (i) a linear term in non-congestion benefits, (ii) an integral term in congestion loads, and (iii) a convex term in SP costs.

D.2 Integral-Pointwise Sandwich Inequality

To relate user-level congestion penalties to the integrated congestion term in the potential, we use a simple ‘‘sandwich’’ inequality for increasing functions.

Proposition 8 (Integral-pointwise sandwich). *Let $\tau_i : [0, \infty) \rightarrow [0, \infty)$ be nonnegative and increasing. For any $y \geq 0$ and any $\gamma_{j,i} > 0$,*

$$\gamma_{j,i} \tau_i(y_i) \leq \int_{y_i}^{y_i + \gamma_{j,i}} \tau_i(z) dz \leq \gamma_{j,i} \tau_i(y_i + \gamma_{j,i}). \quad (54)$$

Sketch. For all $z \in [y_i, y_i + \gamma_{j,i}]$, monotonicity gives $\tau_i(y_i) \leq \tau_i(z) \leq \tau_i(y_i + \gamma_{j,i})$. Integrating over this interval yields (54). Equivalently, by the mean-value theorem for integrals, the integral equals $\gamma_{j,i} \tau_i(\xi)$ for some $\xi \in [y_i, y_i + \gamma_{j,i}]$, which directly implies the bounds. ■

Interpretation. The integral in (54) can be viewed as the average of pointwise congestion penalties between y_i and $y_i + \gamma_{j,i}$. Its sign changes exactly when the pointwise terms do, which is the key to aligning changes in the potential with changes in individual utilities.

For the linear-response model $\tau_i(y) = y/f_i^{\text{On}}$,

$$\int_y^{y+\gamma} \tau_i(z) dz = \frac{(y+\gamma)^2 - y^2}{2f_i^{\text{On}}} = \frac{y\gamma}{f_i^{\text{On}}} + \frac{\gamma^2}{2f_i^{\text{On}}}, \quad (55)$$

so the integrated congestion level is $(y + \frac{\gamma}{2})/f_i^{\text{On}}$, which lies between $\tau_i(y)$ and $\tau_i(y + \gamma)$.

D.3 Single-User Deviation: Utility and Potential Changes

We next spell out the single-user deviation that underlies the ordinal-potential proof. The goal is to compare the sign of the utility change with that of the potential change.

Deviation setup. Fix an action profile $\boldsymbol{\pi}$ and SD u_j^{On} . Consider a unilateral deviation

$$\pi_j = i \rightarrow \pi'_j = i', \quad \boldsymbol{\pi}' = (\boldsymbol{\pi}_{-j}, i'). \quad (56)$$

By (20), the congestion loads at the two involved SPs satisfy

$$y_{i'}(\boldsymbol{\pi}') = y_{i'}(\boldsymbol{\pi}) + \gamma_{j,i'}, \quad (57)$$

$$y_i(\boldsymbol{\pi}') = y_i(\boldsymbol{\pi}) - \gamma_{j,i}. \quad (58)$$

The corresponding physical workloads evolve as

$$x_{i'}(\boldsymbol{\pi}') = x_{i'}(\boldsymbol{\pi}) + r_j, \quad \mathbf{x}_i(\boldsymbol{\pi}') = \mathbf{x}_i(\boldsymbol{\pi}) - r_j. \quad (59)$$

Utility change. Using the unified utility (19), the change in SD u_j^{On} 's utility is

$$\begin{aligned} \Delta U_j &= U_{j,i'} - U_{j,i} \\ &= \left(S_j(i') - S_j(i) \right) - \kappa_j \theta_{j,i'} \tau_{i'}(y_{i'}(\boldsymbol{\pi}')) + \kappa_j \theta_{j,i} \tau_i(y_i(\boldsymbol{\pi})) \\ &\quad - (p_{j,i'} - p_{j,i}). \end{aligned} \quad (60)$$

The first term is the change in non-congestion benefit, the next two terms capture the congestion effect, and the last term is a pure payment transfer.

Potential change. By (21), the potential change is

$$\begin{aligned} \Delta \Phi &= \Phi(\boldsymbol{\pi}') - \Phi(\boldsymbol{\pi}) \\ &= \underbrace{S_j(i') - S_j(i)}_{\text{non-congestion benefit}} \\ &\quad - \underbrace{\left(\int_{y_{i'}(\boldsymbol{\pi})}^{y_{i'}(\boldsymbol{\pi}) + \gamma_{j,i'}} \tau_{i'}(z) dz - \int_{y_i(\boldsymbol{\pi}) - \gamma_{j,i}}^{y_i(\boldsymbol{\pi})} \tau_i(z) dz \right)}_{\text{integrated congestion variation}} \\ &\quad - \underbrace{\left(K_{i'}(x_{i'}(\boldsymbol{\pi}) + r_j) - K_{i'}(x_{i'}(\boldsymbol{\pi})) \right)}_{\text{SP } i' \text{ cost increase}} \\ &\quad + \underbrace{\left(K_i(\mathbf{x}_i(\boldsymbol{\pi})) - K_i(\mathbf{x}_i(\boldsymbol{\pi}) - r_j) \right)}_{\text{SP } s_i^{\text{On}} \text{ cost decrease}}. \end{aligned} \quad (61)$$

Payment terms are absent from $\Delta \Phi$ by construction (see Appx. D.9).

D.4 Approximate Linearization of Soft-Deadline Utility

We briefly justify the linearized MU utility in (18) and the definition of the congestion-sensitivity coefficient κ_j .

Recall that for MU u_j^{On} offloading to s_i^{On} ,

$$G_{j,i}^{\text{M}} = v_j \frac{[\tau_j^{\text{ddl}} - T_{j,i}^{\text{edge}}]_+}{\tau_j^{\text{ddl}}}, \quad T_{j,i}^{\text{edge}} = t_{j,i}^{\text{comp}} + t_{j,i}^{\text{tx}}. \quad (62)$$

In the practically relevant regime where $T_{j,i}^{\text{edge}} \lesssim \tau_j^{\text{ddl}}$, the operator $[\cdot]_+$ is active and

$$G_{j,i}^{\text{M}} = v_j - v_j \frac{t_{j,i}^{\text{tx}}}{\tau_j^{\text{ddl}}} - v_j \frac{t_{j,i}^{\text{comp}}}{\tau_j^{\text{ddl}}}. \quad (63)$$

Using $t_{j,i}^{\text{comp}} = \theta_{j,i} \tau_i(y_i)$, we obtain

$$G_{j,i}^{\text{M}} = \underbrace{v_j - v_j \frac{t_{j,i}^{\text{tx}}}{\tau_j^{\text{ddl}}}}_{\text{independent of } y_i} - \underbrace{v_j \frac{\theta_{j,i}}{\tau_j^{\text{ddl}}}}_{\text{congestion-dependent term}} \tau_i(y_i). \quad (64)$$

Adding the energy-saving term $c_{j,i}^{\text{M,save}} = E_{j,i}^{\text{loc}} - E_{j,i}^{\text{tx}}$ with coefficient \mathbb{V}_e^{M} and subtracting the payment, the full MU utility can be written as

$$U_{j,i}^{\text{M}} = \tilde{S}_j(i) - \kappa_j \theta_{j,i} \tau_i(y_i) - p_{j,i}, \quad (65)$$

where

$$\tilde{S}_j(i) = v_j - v_j \frac{t_{j,i}^{\text{tx}}}{\tau_j^{\text{ddl}}} + \mathbb{V}_e^{\text{M}} c_{j,i}^{\text{M,save}}, \quad \kappa_j = \frac{v_j}{\tau_j^{\text{ddl}}} > 0. \quad (66)$$

Thus, MUs share the same congestion structure as HUs, with user-specific κ_j . This linearization preserves the *ordinal* ranking of actions induced by the original soft-deadline utility in the operating regime of interest, and hence does not change the set of NE.

D.5 Sign Consistency of Congestion Terms

The ordinal-potential property relies on the fact that congestion terms in the utility and in the potential move in the same direction.

Proposition 9 (Sign consistency). *For deviation $\pi_j : i \rightarrow i'$, the congestion part of the utility change,*

$$-\kappa_j \theta_{j,i'} \tau_{i'}(y_{i'}(\boldsymbol{\pi}')) + \kappa_j \theta_{j,i} \tau_i(y_i(\boldsymbol{\pi})),$$

and the congestion-integral term in the potential change,

$$-\left(\int_{y_{i'}(\boldsymbol{\pi})}^{y_{i'}(\boldsymbol{\pi})+\gamma_{j,i'}} \tau_{i'}(z) dz - \int_{y_i(\boldsymbol{\pi})-\gamma_{j,i}}^{y_i(\boldsymbol{\pi})} \tau_i(z) dz \right),$$

have the same sign.

Proof. Apply Proposition 8 to both integrals. Each integral lies between a lower and an upper pointwise congestion term. After scaling by the positive factors $\kappa_j \theta_{j,i} / \gamma_{j,i}$ and $\kappa_j \theta_{j,i'} / \gamma_{j,i'}$, the corresponding bounds match the pointwise expressions in the lemma. Hence the two congestion components must share the same sign. ■

For the linear model $\tau_i(y) = y/f_i^{\text{On}}$, the result is even more transparent: the integral is simply the area under a straight line, so shifting traffic to a more congested SP increases both the user's delay and the integrated congestion cost.

D.6 Monotonicity and Convexity of SP Cost

The SP-cost term $K_i(\cdot)$ is chosen to discourage load concentration on heavily utilized SPs.

Assume $K_i : \mathbb{R}_+ \rightarrow \mathbb{R}_+$ is increasing and convex. Then for $x'_i = x_i - r_j$ and $x'_i = x_i + r_j$,

$$K_{i'}(x_i + r_j) - K_{i'}(x_i) \geq 0, \quad K_i(x_i) - K_i(x_i - r_j) \geq 0. \quad (67)$$

Convexity further implies that the marginal cost $K_i(x + \Delta) - K_i(x)$ is nondecreasing in x : adding the same workload to a more congested SP incurs a larger cost. Consequently,

$$-\left[K_{i'}(x_i + r_j) - K_{i'}(x_i) \right] + \left[K_i(x_i) - K_i(x_i - r_j) \right] \quad (68)$$

moves in a direction consistent with the deviation: shifting load towards a more congested SP is penalized in the potential.

For the linear model $K_i(x) = \omega_1 e_i^{\text{comp}} x / f_i^{\text{On}}$, these increments are simply proportional to r_j and preserve the sign.

D.7 Proof Sketch of Proposition 7

We are now ready to justify the ordinal-potential property.

Consider a deviation $\pi_j : i \rightarrow i'$ that strictly increases SD u_j^{On} 's utility, i.e., $\Delta U_j > 0$ in (60). Comparing (60) and (61), we note:

- The non-congestion term $S_j(i') - S_j(i)$ appears identically in both ΔU_j and $\Delta \Phi$.
- By Proposition 9, the congestion contributions to ΔU_j and $\Delta \Phi$ have the same sign.

- By Appx. D.6, the SP-cost variation responds monotonically and convexly to the direction of load shift, further aligning the sign of $\Delta \Phi$ with that of ΔU_j .
- Payment differences $-(p_{j,i'} - p_{j,i})$ only redistribute welfare and are excluded from $\Delta \Phi$ (Appx. D.9), so they do not affect the ordinal comparison.

Hence, $\Delta U_j > 0$ implies $\Delta \Phi > 0$, which proves that $\Phi(\boldsymbol{\pi})$ is an *ordinal* potential for the considered game, as stated in Proposition 7.

D.8 Finite-Improvement Property and Existence of NE

The ordinal-potential property directly yields convergence of better-response dynamics and existence of pure-strategy Nash equilibria.

Let $\mathcal{A}_j = \{0\} \cup \mathcal{S}^{\text{On}}$ be SD u_j^{On} 's finite action set, and $\mathcal{A} = \prod_j \mathcal{A}_j$ the joint action space. Consider any strict better-response dynamics in which, at each step, some SD switches to an action that strictly improves its utility. By Proposition 7, every such deviation strictly increases the potential $\Phi(\boldsymbol{\pi})$.

Since \mathcal{A} is finite, the sequence of potential values cannot increase indefinitely. The process must terminate after finitely many steps at a profile $\boldsymbol{\pi}^*$ where no SD can further increase its utility via a unilateral deviation. By definition, $\boldsymbol{\pi}^*$ is a pure-strategy NE. Moreover, any local maximizer of $\Phi(\boldsymbol{\pi})$ is a pure-strategy NE, because any unilateral move would reduce (or not increase) Φ , and hence would not increase the deviator's utility in an ordinal-PG.

This finite-improvement property underpins PG-BRD: as long as SDs occasionally update their actions based on best responses, the algorithm converges in finitely many steps to a stable congestion-aware offloading configuration.

D.9 Treatment of Monetary Payments in the Potential Function

We finally clarify why monetary payments are left out of the potential, which is sometimes questioned from a mechanism-design perspective.

Let $\mathcal{W}(\boldsymbol{\pi})$ denote the *non-transfer* welfare:

$$\mathcal{W}(\boldsymbol{\pi}) = \sum_{j: \pi_j \neq 0} S_j(\pi_j) - \sum_i \int_0^{y_i(\boldsymbol{\pi})} \tau_i(z) dz - \sum_i K_i(x_i(\boldsymbol{\pi})). \quad (69)$$

Agent-to-agent payments $\{p_{j,i}\}$ are internal transfers between SDs and SPs. In the absence of external taxes or subsidies, they sum to zero at the system level and do not affect $\mathcal{W}(\boldsymbol{\pi})$. Thus, payments can be omitted from the potential without changing ordinal comparisons between profiles.

In other words, $\Phi(\boldsymbol{\pi})$ is designed as a proxy for *real* system efficiency, capturing latency savings, energy savings, congestion, and SP costs, while treating payments as a separate distributional layer superimposed on top of this efficiency metric. This follows standard practice in congestion and resource-allocation games and allows PG-BRD to focus on aligning individual incentives with global performance, independently of how the resulting welfare is split among participants.